Site M0062[1]

T. Andrén, B.B. Jørgensen, C. Cotterill, S. Green, E. Andrén, J. Ash, T. Bauersachs, B. Cragg, A.-S. Fanget, A. Fehr, W. Granoszewski, J. Groeneveld, D. Hardisty, E. Herrero-Bervera, O. Hyttinen, J.B. Jensen, S. Johnson, M. Kenzler, A. Kotilainen, U. Kotthoff, I.P.G. Marshall, E. Martin, S. Obrochta, S. Passchier, N. Quintana Krupinski, N. Riedinger, C. Slomp, I. Snowball, A. Stepanova, S. Strano, A. Torti, J. Warnock, N. Xiao, and R. Zhang[2]

Chapter contents

[1] Andrén, T., Jørgensen, B.B., Cotterill, C., Green, S., Andrén, E., Ash, J., Bauersachs, T., Cragg, B., Fanget, A.-S., Fehr, A., Granoszewski, W., Groeneveld, J., Hardisty, D., Herrero-Bervera, E., Hyttinen, O., Jensen, J.B., Johnson, S., Kenzler, M., Kotilainen, A., Kotthoff, U., Marshall, I.P.G., Martin, E., Obrochta, S., Passchier, S., Quintana Krupinski, N., Riedinger, N., Slomp, C., Snowball, I., Stepanova, A., Strano, S., Torti, A., Warnock, J., Xiao, N., and Zhang, R., 2015. Site M0062. *In* Andrén, T., Jørgensen, B.B., Cotterill, C., Green, S., and the Expedition 347 Scientists, *Proc. IODP,* 347: College Station, TX (Integrated Ocean Drilling Program).
doi:10.2204/iodp.proc.347.106.2015
[2] **Expedition 347 Scientists' addresses.**

Introduction

During Integrated Ocean Drilling Program (IODP) Expedition 347, cores were recovered from four holes at Site M0062 (Ångermanälven River estuary), with an average site recovery of 99%. In addition, two shallow gravity (Rumohr) cores were acquired. The water depth was 69.3 m, with no tidal range. Existing data sets, including seismic reflection profiles, were evaluated prior to each site to attempt to guide the initial drilling with an anticipated lithologic breakdown. The total time spent on station was 1.03 days.

Operations

Transit to Hole M0062A

Operations in Hole M0061C were completed at 1220 h on 5 October 2013. The vessel then awaited the arrival of a pilot at 1600 h before transiting to Hole M0062A (proposed Site BSB-11).

Hole M0062A

The vessel arrived on site at 1810 h on 5 October 2013 and commenced operations, having built the dynamic positioning (DP) model (Table **T1**). The uppermost 0.5 m was not cored because of the potential presence of harmful contaminants associated with historic paper mill outputs. In accordance with the risk assessment, additional personal protective equipment (PPE) was worn for the first core runs at this site.

Eleven piston cores and one hammer sample were collected at this site on 5–6 October. As at Site M0061, the end of the hole was called when drilling encountered the sand lithology underlying the varved sequence. In this hole, the operation was terminated at 35.90 meters below seafloor (mbsf), and the vessel prepared to move over to Hole M0062B.

A total of 12 coring attempts were made in Hole M0062A, along with one open-hole section at the surface (to avoid coring contaminated sediments). The maximum hole depth was 35.90 mbsf with a recovery of 97.41% (inclusive of the open-hole 0.5 m) and 97.82% when the open-hole interval is removed from the calculation.

doi:10.2204/iodp.proc.347.106.2015

Hole M0062B

The vessel established position over Hole M0062B at 0423 h on 6 October 2013. The noncoring assembly (NCA) was again used for the uppermost 1 m because of the potential for contamination and to establish the offset between core runs required to produce a composite stratigraphy for this site.

Piston coring ran smoothly throughout 6 October using seawater as the drill fluid. The hole ended at 24.10 mbsf in silty material.

A total of seven cores (and one 1 m NCA section) were attempted in Hole M0062B. Hole recovery was 98.57% when the open-hole section is discounted.

Hole M0062C

After coring Holes M0062A and M0062B, it was possible to reassess the risk of coring contaminated sediments. It was evaluated on board whether any risk from collecting a surface piston core could be mitigated and decided that scientifically it would be beneficial to provide this uppermost interval.

One core was collected from this hole. This core recovered 3.43 m of sediment from a 3.3 m run, indicating expansion.

Hole M0062D

At 1000 h on 6 October 2013, the vessel established position over Hole M0062D. The uppermost 1.5 m of sediment was not cored in order to establish the offset between core runs required to produce a composite stratigraphy using all holes at this site. The NCA was initially used before switching to the piston corer system for the remainder of the hole. The first core was recovered to deck at 1025 h. Coring ran smoothly on 6 October, and the final core was recovered to deck at 1405 h, after which the drill floor was prepared for downhole logging.

Downhole logging operations were run by the Petrophysics Staff Scientist and the Weatherford Engineer and Technician. Setup for logging operations was complete at 1535 h, and the first tool string was run shortly afterward. The string consisted of the compact gamma ray and compact induction tools. The first uplog began at 1600 h, and the tool reached 9.50 mbsf, when the string lost tension. The tool was recovered to deck at 1610 h. The second logging run involved the compact gamma ray and compact spectral gamma tools and was run into the hole at 1625 h. Again, the string lost tension at 9.50 mbsf and the uplog began at 1634 h. The tool was then recovered on deck. Because of the short section of hole that remained open for logging, logging operations ended after this run, and the vessel prepared for transit to Site M0063.

Seven cores were recovered in this hole to 21.0 mbsf, with a recovery of 100%. An open-hole section of 1.5 m was drilled.

Holes M0062K and M0062L

Two Rumohr cores were also collected at this site on 6 October 2013, following a reassessment of the potential risk from coring contaminated sediments in the upper 50 cm. The corer was deployed over the starboard side of the vessel using a system of winches. The corer recovered 0.95 m (Hole M0062K) and 0.92 m (Hole M0062L) of sediment. In order to mitigate any risk from contaminated sediment associated with the historical paper mill industry, additional PPE was used by those involved in acquiring the Rumohr cores. The Rumohr corer and outside of the liner were pressure washed prior to being brought onto the vessel to remove as much potentially contaminated material as possible. All equipment and PPE were also thoroughly washed after use. The cores themselves were labeled and sealed in black bags for transport back to the IODP Bremen Core Repository (Germany).

Lithostratigraphy

Six holes were drilled at Site M0062: Hole M0062A to a total depth of 35.9 mbsf, Hole M0062B to 24.1 mbsf, Hole M0062C to 3.3 mbsf, and Hole M0062D to 21.0 mbsf. Holes M0062K and M0062L were Rumohr cores (<1 m penetration gravity cores) designated for microbiology and paleoceanographic sampling. These cores were not included in the core description at the IODP Bremen Core Repository. Expansion of cores and gas release on recovery resulted in variable core quality in the upper ~15 mbsf. Lithostratigraphic divisions (Units I and II; Fig. **F1**) are based on descriptions made on the cut face of the split core and observations from smear slides (see **"Core descriptions"**).

Unit I

Subunit Ia

Intervals: 347-M0062A-2H-1, 0 cm, to 5H-1, 32 cm; 347-M0062B-2H-1, 0 cm, to 5H-1, 0 cm; 347-M0062C-1H-1, 0 cm, to end of hole; 347-M0062D-2H-1, 0 cm, to 4H-2, 100 cm

Depths: Hole M0062A = 0–10.72 mbsf; Hole M0062B = 0–10.90 mbsf; Hole M0062C = 0–3.30 mbsf; Hole M0062D = 0–10.60 mbsf

Subunit Ib

Intervals: 347-M0062A-5H-1, 32 cm, to 6H-2, 97 cm; 347-M0062B-5H-1, 0 cm, to 6H-3, 0 cm; 347-M0062D-4H-2, 100 cm, to 6H-2, 88 cm

Depths: Hole M0062A = 10.72–16.17 mbsf; Hole M0062B = 10.90–17.09 mbsf; Hole M0062D = 10.60–17.08 mbsf

Unit I comprises very dark greenish gray laminated silty clay. Laminae consist of horizontal, planar, and parallel couplets of light and dark laminae. Subunit Ia is laminated on a millimeter scale and contains two distinct 0.5–1 m thick greenish black intervals between ~6 and 8.5 mbsf. The upper interval has a diffuse top and a sharp bottom at 6.3 mbsf at Sections 347-M0062A-3H-2, 100 cm, and 347-M0062B-3H-2, 50 cm, and at 6.45 mbsf at Section 347-M0062D-3H-2, 15 cm. The lower interval has a sharp top at 7.74–8.03 mbsf at Sections 347-M0062A-4H-1, 83 cm, 347-M0062B-4H-1, 14 cm, and 347-M0062D-3H-CC, 0 cm, and a diffuse bottom. Interlaminated "varve-like" silty clay–clay couplets are observed in Subunit Ib, with light-colored silty clay grading upward into clay within each couplet (Fig. F2). The bottom of Unit I is defined based on the first downcore appearance of sand interbeds. A gradual upcore decrease in couplet thickness is observed within Subunit Ib: couplet thicknesses are 4–10 cm immediately above the Unit I/II boundary, decreasing upcore to 3–4 mm over a ~2 m interval (Fig. F2).

The couplets in Unit I, and especially Subunit Ib, have characteristics of glacial lake varves. In estuaries, rhythmites can also result from tidal processes; however, the tidal range in the Baltic Sea is negligible. The boundary between Subunits Ia and Ib may mark a transition from lacustrine to brackish-marine conditions in the Ångermanälven River estuary. The greenish black intervals comprise iron sulfide precipitates, likely resulting from diagenetic activity after deposition and preservation of organic matter from a stratified water column.

Unit II

Intervals: 347-M0062A-6H-2, 97 cm, to end of hole; 347-M0062B-6H-3, 0 cm, to end of hole; 347-M0062D-6H-2, 88 cm, to end of hole

Depths: Hole M0062A = 16.17–35.90 mbsf; Hole M0062B = 17.09–24.10 mbsf, Hole M0062D = 17.08–21.00 mbsf

Unit II comprises a well-sorted dark gray fine to medium sand. The upper part includes several fining-upward sequences from medium sand to silt (interval 347-M0062A-7H-1, 93 cm, to 7H-2, 150 cm) as thick as 60 cm, as well as silt laminae and silt interbeds. Toward the base, the unit is dominated by homogeneous beds of fine and medium sand. High mica and opaque mineral contents are observed throughout Unit II.

The coarse-grained nature of the sediment and the fining-upward beds suggest that this unit was deposited as a result of traction transport in a glaciofluvial, fluvial, or tidal system, although the latter is unlikely because of the nontidal regime of the Baltic Sea. The fining-upward units probably indicate glaciofluvial or fluvial channel deposits.

Biostratigraphy

Diatoms

Qualitative analysis of diatom community composition was carried out on 18 samples from Hole M0062A. Samples were taken with a spacing of 1.5 m or less in the upper 8.6 mbsf of the core and at every core top for the remainder. Diatoms were identified to species level (Tables T2, T3), and chrysophyte cysts were assigned to morphotypes and present at all analyzed intervals. Diatom taxa were classified with respect to salinity tolerance into five groups (fresh, brackish-fresh, brackish, brackish-marine, and marine) as well as life forms (planktonic, periphytic, and sea ice) according to the Baltic Sea intercalibration guides of Snoeijs et al. (1993–1998). Paleoecological information is illustrated in Figure F3. Although quantitative preservational analysis is yet to be completed, diatom preservation is generally considered to be of high quality based on the presence of gracile taxa.

0–3.4 mbsf

This interval contains mainly freshwater taxa from the planktonic genera *Aulacoseira* and *Cyclotella* and the periphytic genera *Gomphonema* and *Tabularia*. Some brackish-freshwater taxa (e.g., *Diatoma vulgaris*) and brackish taxa (e.g., *Cyclotella choctawhatcheeana*) are also present at low abundances. Sea ice affiliated taxa are not present in this interval. This assemblage represents a very low salinity environment and contains freshwater taxa both from the Ångermanälven River and lake associated freshwater taxa. Notably, *Chaetoceros* resting spores are not present, implying very low photic zone salinity throughout this interval.

3.4–7.1 mbsf

This interval contains a relatively higher concentration of brackish and brackish-marine taxa, specifically *Rhoicosphenia curvata*, *Thalassiosira levanderi*, and *Chaetoceros* resting spores. Additionally, the sea ice associated taxon *Pauliella taeniata* is present in

this interval. This species is known to occur across the Baltic Sea during the spring bloom following winters with extensive sea ice cover (Hajdu et al., 1997; Hasle and Syvertsen, 1990; Snoeijs, 1993–1998; Weckström and Juggins, 2006). *Chaetoceros* is associated with high-productivity water columns (e.g., Leventer, 1992; Andrén et al., 2000). This interval is interpreted as a brackish estuarine environment with input of freshwater from the Ångermanälven River. The lowermost part of this interval, from 6.8 to 7.1 mbsf, documents the transition from a freshwater environment below to an estuarine environment above.

7.1–8.6 mbsf

This interval contains mainly freshwater taxa, including many large lake-associated taxa (e.g., *Stephanodiscus neoastraea* and a diverse *Aulacoseira* assemblage). Brackish and brackish-marine taxa are very rare. This interval is interpreted as a large lake setting with minor brackish water influence.

8.6 mbsf and deeper

This interval is devoid of siliceous microfossils.

Foraminifers and ostracods

A total of 17 offshore and 5 onshore samples were prepared for foraminiferal and ostracod analysis from Site M0062. No foraminifers or ostracods were found at this site. The lack of foraminifers suggests that conditions during the entire period represented by these cores were too fresh to support foraminifers. Very few microfossils >63 µm are present. Cladoceran antennae occur occasionally and testate amoebae occur very rarely in the upper 10 mbsf, suggesting a freshwater environment. A blue precipitate presumed to be vivianite occurs in Section 347-M0062A-3H-1, suggesting degradation of organic matter in the presence of abundant dissolved iron.

Palynological results

For Site M0062, palynological analyses focused on Holes M0062A and M0062B (see PalyM0062.xls in PALYNOLOGY in **"Supplementary material"**). Generally, one sample per core was examined for palynomorphs. The present-day regional vegetation in the area is dominated by pine (*Pinus*), birch (*Betula*), and spruce (*Picea*) trees.

Hole M0062A

From Hole M0062A, 10 sediment samples (from Cores 347-M0062A-3H through 8H, two sections from Core 10H, and Cores 11H and 13H) were analyzed. Only the uppermost two samples contain enough palynomorphs to produce statistically relevant results (90,000 to 120,000 grains/cm^3). Samples from Cores 5H and 6H contain pollen in very low concentrations. Samples from Cores 7H, 8H, 10H, 11H, and 13H are virtually barren of palynomorphs. In the following sections, results for the samples from Cores 3H and 4H are described and discussed in combination with results from neighboring Hole M0062B.

Hole M0062B

From Hole M0062B, six sediment samples (Cores 347-M0062B-2H through 7H) were analyzed. The uppermost four samples contain enough palynomorphs to generate statistically relevant results. Cores 2H through 4H (1.23–7.70 mbsf), in particular, contain very well preserved palynomorphs, mainly of terrestrial origin (Figs. **F4, F5**), whereas marine palynomorphs are rare. The pollen concentration varies between 100,000 and 240,000 grains/cm^3 for Cores 2H through 4H; in the sample from Core 5H (11.23 mbsf), the concentration is only ~6400 grains/cm^3.

1.23–14.35 mbsf

The pollen diagram (Fig. **F6**) from Site M0062 (Holes M0062A and M0062B spliced) is divided into two phases, with five pollen spectra from 1.23 to 7.70 mbsf reflecting the Holocene and only one sample (11.23 mbsf) representing the onset of the Holocene. The most characteristic element of the pollen spectra from the uppermost three samples investigated (samples at 4.39, 4.22, and 1.23 mbsf) is the occurrence of *Picea* pollen. The percentage of the *Picea* pollen in these samples amounts to 13%, 16%, and 9%, respectively. In northern central Sweden, such high amounts of *Picea* pollen are noted between 3000 and 2500 cal y BP in lacustrine sediments (Antonsson et al., 2006; Wallin, 1996). In pollen spectra at 7.45 and 7.70 mbsf, the amounts of *Pinus sylvestris* type pollen are only 31%–41%, whereas those of *Betula alba* type increase to 40%–42%. Also, the percentage of *Alnus glutinosa* type pollen increases to 12.5%. Pollen of other thermophilous deciduous trees also occur, with *Quercus* and *Ulmus* pollen percentages reaching 4%. *Fraxinus* pollen are present, too. All the above may suggest a mid-Holocene age for the sediment interval.

For nonpollen palynomorphs, the uppermost sample is characterized by particularly frequent *Cosmarium* freshwater algae. This genus also occurs in other samples from Site M0062 and, together with regular occurrences of *Botryococcus* and *Pediastrum*, indicates strong freshwater input or lacustrine conditions. Lacustrine conditions are also implied by occurrences

of aquatic insect larvae in Cores 347-M0062B-3H and 5H (4.34 and 11.23 mbsf). Two jaws could be identified as chironomid remains (one from a member of Tanytarsini and one from *Corynoneura*; Fig. F4). Cores 347-M0062B-2H through 4H (1.23–7.70 mbsf) also contain several Thecamoebae remains.

The oldest level characterized by the pollen spectra is represented by a single pollen spectrum at 11.23 mbsf. This pollen spectrum is dominated by pioneer tree species *Pinus sylvestris* type (74%) and *Betula alba* type (14%). Among pollen from other trees, pollen of *Alnus glutinosa* type (5.5%) and *Ulmus* (1%) was noted. Nonarboreal pollen is represented by *Artemisia* (2%), Poaceae (1%), and Chenopodiaceae (1%). Compared to the high-resolution pollen record from Lake Gilltjärnen in northern central Sweden (Antonsson et al., 2006), this pollen spectrum may be provisionally ascribed to the onset of the Holocene. This suggestion may be endorsed by the presence of the above-mentioned herb pollen (i.e., *Artemisia* and Chenopodiaceae). Pollen of these taxa are related to open plant communities, most of which were probably of importance during the early Holocene.

Marine dinocysts and other marine palynomorphs are extremely rare in all samples from Site M0062, except for a few occurrences of *Operculodinium centrocarpum*/*Protoceratium reticulatum* with short processes. This underlines the similarity to the palynomorph record from Site M0061. Tintinnid remains were encountered in Core 347-M0062B-2H (Fig. F4).

Geochemistry

The geochemical concentration profiles at Site M0062, which is located in the Ångermanälven River inner estuary, are very similar to those of Site M0061 and reflect the strong temporal variations in depositional conditions (see "Lithostratigraphy" and "Biostratigraphy").

Interstitial water

Salinity variations: chloride, salinity, and alkalinity

Chloride (Cl^-) concentrations increase from ~90 to 150 mM from the top to the bottom of the 35.9 m drilled sequence (Fig. F7A). Calculated salinities based on Cl^- concentrations ("Cl^- based salinity") are consistent with the shipboard salinity, and both range ~6–10 (Fig. F7B–F7C; Table T4). The higher salinities at depth suggest that bottom water salinity was higher in the past than it is at present, corroborating observations at Sites M0059, M0061, and M0063. Alkalinity initially increases with depth and reaches a maximum of 22 meq/L at ~5 mbsf before gradually decreasing downhole to ~6 meq/L (Fig. F7D). The salinity and alkalinity profiles are very similar in magnitude and trend to those observed at Site M0061.

Organic matter degradation: sulfate, sulfide, ammonium, phosphate, iron, manganese, pH, bromide, and boron

Sulfate (SO_4^{2-}) concentrations are typically <0.1 mM to ~16 mbsf (Fig. F8A). Deeper SO_4^{2-} concentrations gradually increase to ~5 mM at the bottom of the profile. Sulfide (H_2S) concentrations are below detection throughout the sediment column (Fig. F8B).

Ammonium (NH_4^+) and phosphate (PO_4^{3-}) concentrations both reveal peaks near 7 mbsf, slightly deeper that of alkalinity, with peak values of ~0.9 and 0.3 mM, respectively (Fig. F8C–F8D). However, PO_4^{3-} concentrations sharply decrease to 0.02 mM to 13 mbsf, whereas NH_4^+ gradually declines to 0.17 mM at the base of the profile. Together, the elevated values for alkalinity, NH_4^+, and PO_4^{3-} provide evidence for microbial remineralization of organic matter as a more active process in the upper ~10 m of the profile.

Dissolved iron (Fe^{2+}) concentrations sharply decrease from ~1100 µM near the surface to 10 µM by 7.5 mbsf (Fig. F8E). Deeper concentrations again rise to a peak of 400 µM centered at ~13 mbsf before declining to ~34 µM by the bottom of the section. Manganese (Mn^{2+}) concentrations decrease from ~800 µM to near 90 µM by 10 mbsf, have a broad maximum around 15–20 mbsf (~220 µM), and further decline to near 50 µM by the bottom of the hole (Fig. F8F). Trends in pore water Fe^{2+} and Mn^{2+} are similar to those observed at Site M0061, although absolute concentrations at Site M0062 are higher. pH shows an increase in the upper 7.5 mbsf to a maximum of ~8.4, followed by a decline to 7.9 at ~15 mbsf, and then again a gradual rise deeper than this depth (Fig. F8G).

The profile of bromide (Br^-) shows a similar trend to that of salinity (Fig. F9A). As for Site M0061, a slight increase in the Br/Cl ratio relative to that of seawater is observed in the upper ~5 m of the sediment (Fig. F9B). Boron (B) concentrations show a maximum of ~140 µM at 7.5 mbsf and then decrease downhole to values <3 µM at ~20 mbsf before they slightly increase again in the lowermost part of the profile (Fig. F9C). Similar to Site M0061, B/Cl ratios show a maximum in the upper 8 mbsf of the profile with values clearly above the ratio of seawater, suggesting release from the solid phase (Fig. F9D).

Mineral reactions

Sodium, potassium, magnesium, and calcium

Sodium (Na^+) concentrations increase with depth from ~70 to ~120 mM in the upper 10 m of the sediment and then remain relatively constant (Fig. F10A). Potassium (K^+) and magnesium (Mg^{2+}) concentrations both increase in the upper 7–10 mbsf and then decline to 17.5 mbsf before increasing again (Fig. F10B–F10C). Calcium (Ca^{2+}) concentrations gradually increase from near 3 to ~22 mM by 20 mbsf and then remain high to the bottom of the profile (Fig. F10D). Concentrations of Na^+ normalized to Cl^- are close to seawater values all the way down the profile, although with some scatter (Fig. F10E). Ratios of K/Cl suggest release of K^+ in the upper ~8–10 m of the sediment and removal deeper than that interval (Fig. F10F). Ratios of Mg/Cl are nearly constant and near seawater throughout the profile (Fig. F10G), but those of Ca/Cl increase with depth and are consistently above seawater ratios, suggesting release of Ca^{2+} from solids at depth (Fig. F10H). The trends in K^+, Mg^{2+}, and Ca^{2+} at Site M0062 are very similar to those for Site M0061; however, the Na^+ profile is distinctly different. Whereas Na^+ concentrations decrease with depth at Site M0061, they are relatively constant deeper than ~10 mbsf at Site M0062.

Strontium, lithium, dissolved silica, and barium

Strontium (Sr^{2+}), lithium (Li^+), barium (Ba^{2+}), and dissolved silica (H_4SiO_4) profiles are very similar to those for Site M0061. Strontium concentrations increase with depth from ~20 to ~50 µM (Fig. F11A). Lithium concentrations show a maximum of 6 µM around ~6 mbsf (Fig. F11B). Deeper concentrations decrease to ~3 µM around 10 mbsf and then increase again to ~8 µM by 20 mbsf. Barium concentrations are near 1 µM to 6 mbsf and then sharply rise to a peak of 18 µM around 15 mbsf (Fig. F11C). Deeper Ba^{2+} values drop back to near 1 µM at 20 mbsf. Dissolved silica concentrations increase from the surface to a peak at ~800 µM over the uppermost 8 m of the sediment (Fig. F11D) and then decline to 300–400 µM after passing through a minimum of ~250 µM at 12 mbsf. The higher H_4SiO_4 concentrations in the upper ~8 m correlate well with the occurrence of diatoms in these layers, suggesting potential dissolution of siliceous microfossils (see **"Biostratigraphy"**).

Molybdenum, vanadium, and titanium

Pore water molybdenum (Mo) concentrations show a maximum of ~0.6 µM between 10 and 15 mbsf (Table T5). The profile is very similar to that of Site M0061, but maximum concentrations are a factor of 3 higher. Vanadium (V) concentrations decline from ~0.2 µM at the surface to ~0.05 µM by 10 mbsf (Table T5). This same trend and similar concentrations are also observed at Site M0061. Concentrations of titanium (Ti) decrease from near 0.2–0.3 µM at the surface to below detection at 10 mbsf (Table T5) with a profile that is very similar to that of Site M0061.

Sediment

Carbon content

The amount of total carbon (TC) in sediments recovered from Site M0062 varies from 0.11 to 2.03 wt% (Fig. F12A; Table T6). The total organic carbon (TOC) content ranges from 0.06 to 1.86 wt% with elevated concentrations (average = 1.06 wt%) present in the uppermost 11 m of the cored sequence (Fig. F12B), roughly coinciding with the gray laminated silty clays of lithostratigraphic Subunit Ia. The pronounced maximum (1.86 wt%) in TOC at 7.4 mbsf seems to be related to the presence of a distinct black interval containing iron sulfide precipitates (see **"Lithostratigraphy"**). Deeper than ~17 mbsf and therefore associated with the first occurrence of the fine to medium sands of Unit II, TOC contents remain uniformly low with values <0.1 wt%.

The total inorganic carbon (TIC) content of sediments from Site M0062 stays low throughout the cored sequence and ranges from below detection to 0.17 wt% (Fig. F12C; Table T6). TIC thus constitutes only a minor component (on average 0.07 wt%) of the total carbon pool preserved in sediments of Site M0062. Similar trends in TIC are observed in Holes M0062A, M0062B, and M0062D, whereas notably lower values are found to occur in Hole M0062B.

Sulfur content

Total sulfur (TS) concentrations generally show little variation with depth and average 0.13 wt% (Fig. F12D; Table T6). An exception is found in the depth interval between 6 and 9 mbsf, which is characterized by two greenish black layers with frequent iron sulfide banding (see **"Lithostratigraphy"**), in which TS values increase to >1 wt% across all holes.

Physical properties

This section summarizes the preliminary physical property results from Site M0062. Four holes were drilled at this site. Hole M0062A was drilled to 35.9 mbsf, Hole M0062B to 24.1 mbsf, Hole M0062C to 3.3 mbsf, and Hole M0062D to 21.0 mbsf. Expansion of cores and gas release resulted in variable core quality in the upper ~15 mbsf. Hole M0062A is the longest and therefore is used to demonstrate the vari-

ability in the physical properties at Site M0062 (Fig. F13). Although all physical property measurements described in "Physical properties" in the "Methods" chapter (Andrén et al., 2015a) were conducted for Site M0062, discrete *P*-wave and thermal conductivity data are too sparsely distributed to exhibit any discernable downcore trend. Noncontact electrical resistivity data also show little variability.

Natural gamma ray, shipboard magnetic susceptibility, and *P*-wave velocity

Natural gamma ray (NGR) exhibits a similar trend as nearby Site M0061 located in the outer Ångermanälven River estuary (Fig. F13) (see "Physical properties" in the "Site M0061" chapter [Andrén et al., 2015b]). NGR increases progressively throughout Subunit Ia and reaches a maximum of ~20 cps at ~11 mbsf at the Subunit Ia/Ib boundary. NGR then progressively decreases to ~10 cps toward the base of Subunit Ib and remains relatively constant (~10 cps) through all of Unit II. Magnetic susceptibility is relatively constant in the upper ~6 m and then exhibits several intervals of increased variability, particularly at ~8–10 mbsf and deeper than ~25 mbsf. Variability in magnetic susceptibility in Unit II might reflect fining-upward sequences from sand to silt (see "Lithostratigraphy" and "Paleomagnetism"). Stepwise increases in baseline magnetic susceptibility values occur at ~8 mbsf and again at ~13.5 mbsf, just below the transition from Subunit Ia and Ib. Conversely, shipboard *P*-wave data are most variable within Subunit Ia. Deeper than ~12 mbsf, *P*-wave velocity is generally high (~1600 m/s) throughout Subunit Ib and Unit II. Through Subunit Ia, similar to other sites, *P*-wave values likely exhibit measurement artifacts that are related to liners that were not fully filled with sediment.

Color reflectance

Lithostratigraphic Subunits Ia and Ib and Unit II are distinguished by differing color reflectance trends that are most apparent in the b* parameter (Fig. F13). Within Subunit Ia, b* exhibits a decreasing (more blue) trend from the core top to 6 mbsf, where values abruptly increase and then vary around a mean value of ~2 until the Subunit Ia/Ib boundary. b* increases progressively to ~4.5 (more yellow) toward the base of Subunit Ib. Unit II is characterized by primarily high values (yellow), in excess of 4, with numerous negative (blue) excursions.

Density

Dry density is generally low (~1 g/cm^3) in Subunit Ia, with a positive excursion near the Subunit Ia/Ib boundary (Fig. F13). Values in Subunit Ib are relatively constant (~1.5 g/cm^3). The highest values, up to ~2 g/cm^3, were measured in the upper ~4 m of Unit II (~17–21 mbsf). From ~21 mbsf, density values in Unit II decrease slightly to a mean of ~1.7 g/cm^3 and remain relatively constant to the bottom of the hole.

Gamma density was measured at 1 cm intervals during the offshore phase of Expedition 347 (Fig. F14). Values are relatively well correlated with the discrete bulk density measurements performed during the Onshore Science Party (OSP) (r^2= 0.86; Fig. F15).

Paleomagnetism

Magnetic susceptibility measurements and rudimentary analyses of the natural remanent magnetization (NRM) were made on discrete specimens of known volume and mass (see "Paleomagnetism" in the "Methods" chapter [Andrén et al., 2015a]). A total of 290 discrete samples were taken from Holes M0062A (161 samples), M0062C (40 samples), and M0062D (89 samples) according to the site splice, with a higher density of samples taken in the upper 9 m. Magnetic susceptibility ranges between 0.07 × 10^{-6} and 0.55 × 10^{-6} m^3/kg through the sequence, with the highest value found within Unit II, a well-sorted dark gray fine to medium sand. The lowest values are confined to a 0.5 m thick interval of greenish black/very dark greenish gray laminated silty clay in Subunit Ia (~8.24–7.74 mbsf, Hole M0062A).

The majority of paleomagnetic pilot samples that were recovered from Unit II carried an intense low-coercivity (easily demagnetized) NRM that reached as high as >300 × 10^{-3} A/m, with one outlier at >800 × 10^{-3} A/m. The inclination values obtained from Unit II clustered between 0° and 30°. These scattered data indicate that the glaciofluvial or fluvial environment represented by Unit II did not allow the geomagnetic field to determine the orientation of minerals that acquire magnetic remanence, although it is likely that the mechanical sorting of minerals in this environment has caused enrichment of the relatively dense magnetic component (most likely magnetite). Subunits Ib and Ia are characterized by less intense NRM with medium coercivity (~30–40 mT). The transition from Unit II to Subunit Ib witnesses a reduction in NRM intensity to <200 × 10^{-3} A/m, and the inclination of Subunits Ia and Ib varies around the geocentric axial dipole (GAD) prediction of 74°. Some samples, particularly in the lower part of Subunit Ib, acquired a relatively intense gyroremanent magnetization (GRM) during AF demagnetization,

suggesting the presence of authigenic greigite (Fe_3S_4) (Snowball, 1997).

Discrete sample measurements

A total of 290 discrete samples were obtained from Site M0062, restricted to core sections included in the site splice. Samples were recovered at intervals of ~50 cm from inside the site splice between 35.9 and 9 meters composite depth (mcd). The sampling density in the upper 9 m was increased to 5 cm intervals.

Magnetic susceptibility

The results of the magnetic analyses are shown in Figure **F16.** Magnetic susceptibility (χ), which was normalized to sample mass, ranges between 0.07×10^{-6} and 0.55×10^{-6} m^3/kg within the hole. Samples taken from Unit II and Subunit Ib have χ values that range between 0.15×10^{-6} and 0.55×10^{-6} m^3/kg. Overlying Subunit Ia has χ values that cluster around 0.2×10^{-6} m^3/kg, with the exception of an interval of low χ (0.1×10^{-6} m^3/kg) between 8 and 7.5 mcd. It is notable that the group of samples in the upper 0.35 m from Hole M0062C has low and variable χ.

The scatter plots of sediment wet density against χ and χ against NRM intensity contain sufficient scatter to suggest that the magnetic properties change with depth, probably as a function of grain size and/or magnetic mineralogy.

Natural remanent magnetization and its stability

Results of the pilot sample demagnetization (Fig. **F17**) indicate that the carrier of NRM alters with depth. Three categories can be identified. Category 1, which is typical of Unit II, is characterized by removal of almost half of the NRM intensity by the 5 mT alternating field (AF) with <20% remaining after demagnetization at 20 mT. The residual vector is not stable but trends away from the origin at AF fields >50 mT. Category 2 is common to Unit I and is typified by a single component of NRM that trends toward the origin during AF demagnetization, with ~10% remaining after the application of an AF of 80 mT. Category 3, which includes some samples close to the transition between Unit II and Subunit Ib and the lower half of Subunit Ia reveals curvilinear vectors that preclude the identification of a stable remanence. This behavior is caused by the acquisition of a GRM and is characteristic of greigite (Fe_3S_4) (Snowball, 1997).

Paleomagnetic directions

The directions of the paleomagnetic vectors are illustrated by the inclination data in Figure **F16.** The inclination data derived from Unit II are unreliable as a record of the ancient geomagnetic field because of the considerable scatter within 0° and 30°. At the transition to Subunit Ib, the inclination steepens to approach a GAD prediction (74°) and varies a few degrees through Unit I, with the exception of four outliers. Declination data (not shown in the figure) are highly scattered because of the high latitude of the site and the fact that the cores were not oriented to an azimuth.

The low inclinations and likely presence of a chemical remanent magnetization (CRM) carried by greigite in Unit II do not allow for reconstructions of paleomagnetic secular variation (PSV). The inclination data from Subunit Ia contain secular variability and may contain a relatively high resolution record of PSV that can be used for relative dating purposes.

Stratigraphic correlation

At Site M0062 four holes were drilled: M0062A (35.9 mbsf), M0062B (24.1 mbsf), M0062C (3.3 mbsf), and M0062D (21.0 mbsf). The meters composite depth (mcd) scale for Site M0062 is based on correlation of magnetic susceptibility between holes (Fig. **F18**). In a similar methodology to that used at previous sites, when on location the offset between adjacent holes was monitored by measuring Fast-track magnetic susceptibility (see **"Physical properties"**) from every other core. These data proved to be an efficient tool to monitor and adjust the drilling process in order to maximize core overlap and composite core recovery. Sediment cores were also logged with a standard multisensor core logger (MSCL) to enable more precise hole-to-hole correlation and to construct a composite section for Site M0062 (Fig. **F18**). Before analysis and correlation, all magnetic susceptibility data were cleaned for the top of each section, removing any outliers from the measurements. The depth offsets that define the composite section for Site M0062 are given in Table **T7** (affine table).

Correlation between the susceptibility anomalies/data in Holes M0062A, M0062B, M0062C, and M0062D is good and enabled us to produce a continuous splice record for this site (Table **T8**). The splice was constructed mainly from Holes M0062A and M0062D. Hole M0062C was used in the splice to cover the uppermost part of the sediment column as Holes M0062A and M0062B were open holed in this interval.

The accuracy of the correlation was visually checked using scanned core slab images in Corelyzer software. At Site M0062, correlation was straightforward to 23.56 mcd (Section 347-M0062A-8H-3, 12.8 cm). The lowermost part of Hole M0062A (interval 347-M0062A-9H-1, 7 cm, to 13H-1, 8 cm) was appended in the splice record. No compression or expansion corrections were applied to the data, so offsets within each core are equal for all points. Thus, it is possible that some features are not similarly aligned between holes.

Seismic units

Seismic sequence boundary-sediment core-MSCL log (magnetic susceptibility) correlations are shown in Figure F19. Correlation is based on the integration of seismic/acoustic data and lithostratigraphy (see "Lithostratigraphy"). Two-way traveltime values were calculated for each lithostratigraphic unit boundary using sound velocity values measured offshore and during the OSP (see "Physical properties"; Table T9). Lithostratigraphic units/unit boundaries were examined at these calculated two-way traveltime values to define the extent of agreement between seismic boundaries and actual lithologic and/or physical properties disconformable surfaces. Uncertainties in the time-depth function could have resulted in minor inconsistencies between seismic features, sedimentological observations from the cores, and the MSCL logs.

Seismic Unit I

Two-way traveltime: 0.110 ms
Lithology: laminated silty clay (lithostratigraphic Subunit Ia)
Depths: 0–10.72 mbsf (M0062A), 0–10.9 mbsf (M0062B), 0–3.3 mbsf (M0062C), 0–10.6 mbsf (M0062D)

Unit I ends at the strong reflector below this stratified seismic unit. Two acoustic subunits can be distinguished (namely acoustic Subunits AUIa and AUIb). In the seismic profile, the upper subunit (AUIa) (0 to ~5 mbsf) is characterized by high-amplitude parallel reflectors and the lower subunit (AUIb) (~5–10.72 mbsf) by low-amplitude parallel reflectors. In Subunit AUIa, magnetic susceptibility values measured in sediment cores (see "Physical properties") stay at similar levels. In Subunit AUIb, magnetic susceptibility values are more variable, peaking in the lowermost part of this subunit.

Seismic Unit II

Two-way traveltime: 0.117 ms
Lithology: interlaminated varve-like silty clay–clay couplets (lithostratigraphic Subunit Ib)
Depths: 10.72–16.17 mbsf (M0062A), 10.9–17.09 mbsf (M0062B), 10.6–17.08 mbsf (M0062D)

The top boundary of Unit II is a strong reflector, which could possibly represent a basin-wide erosional surface, probably related to the erosional surface documented at Site M0061. As in Unit I, two acoustic subunits (AUIIa and AUIIb) can be distinguished. The upper subunit (AUIIa) (10.72 to ~13 mbsf) is acoustically relatively structureless, whereas the lower subunit (AUIIb) (~13–16.17 mbsf) is characterized by low-amplitude parallel reflectors. The boundary between these subunits is slightly irregular and probably erosional. Magnetic susceptibility values of this unit increase downcore. The lower boundary of Unit II is characterized by closely spaced dark reflectors, possibly indicating increases in silt and sand content.

Seismic Unit III

Two-way traveltime: 0.144 ms
Lithology: well-sorted fine to medium sand (lithostratigraphic Unit II)
Depths: 16.17–35.9 mbsf (M0062A), 17.09–24.1 mbsf (M0062B), 17.08–21.0 mbsf (M0062D)

Seismic Unit III is in acoustic images characterized by parallel reflectors in an upper part and a lower homogeneous part, and it could potentially be a continuation of the lower acoustic subunit (AUIIb) of Unit II. The acoustic pulse does not penetrate deep into this unit.

Downhole measurements

Logging operations

Downhole logging measurements in Hole M0062D were made after completion of coring to a total depth of 21 m drilling depth below seafloor (DSF). In preparation for logging, the hole was circulated with seawater and the pipe was pulled back to ~2 m wireline log depth below seafloor (WSF).

For downhole logging in Hole M0062D, two tool strings were deployed:

- The gamma ray tool (MCG)/array induction tool (MAI) tool string, measuring natural gamma ray and electrical resistivity, was run from the seafloor to 10.4 m WSF, where an uplog was started.
- The MCG/spectral gamma ray tool (SGS)/sonic sonde (MSS) tool string, measuring total gamma ray and spectral gamma ray, was run from the seafloor to 10.4 m WSF and an uplog was started.

The tools provided continuous and good quality log data.

Logging units

Hole M0062D was divided into two logging units on the basis of the logs (Fig. F20). The uplog was used as the reference to establish the wireline log depth below seafloor depth scale. There is a good correlation between the gamma ray logs of the two different tool strings.

Logging Unit 1: base of drill pipe to 5.1 m WSF

This logging unit is characterized by a generally increasing gamma ray with large fluctuations between the base of the pipe and 3.7 m WSF in both gamma ray and resistivity. No caliper was run in this hole, but these fluctuations are probably due to poor borehole conditions. The resistivity values decrease slightly from 3.7 to 5.1 m WSF.

Logging Unit 2: 5.1–10.4 m WSF

After a sudden drop in gamma ray values at 5.1 m WSF, NGR values again increase to reach a maximum of nearly 120 gAPI at 7.2 m WSF. Deeper than 7.2 m WSF, NGR remains at constant high values of ~100 gAPI. These high natural gamma ray values correspond to the thick greenish black intervals described in lithostratigraphic Subunit Ia (between ~6 and 8.5 mbsf, see "Lithostratigraphy"). Resistivity values are constant in this logging unit, with a slight increase deeper than 8.8 m WSF. Resistivity values are generally very low in this hole, showing limited compaction.

Both logging Units 1 and 2 correspond to lithostratigraphic Unit Ia.

References

Andrén, E., Andrén, T., and Kunzendorf, H., 2000. Holocene history of the Baltic Sea as a background for assessing records of human impact in the sediments of the Gotland Basin. *Holocene,* 10(6):687–702. **doi:10.1191/09596830094944**

Andrén, T., Jørgensen, B.B., Cotterill, C., Green, S., Andrén, E., Ash, J., Bauersachs, T., Cragg, B., Fanget, A.-S., Fehr, A., Granoszewski, W., Groeneveld, J., Hardisty, D., Herrero-Bervera, E., Hyttinen, O., Jensen, J.B., Johnson, S., Kenzler, M., Kotilainen, A., Kotthoff, U., Marshall, I.P.G., Martin, E., Obrochta, S., Passchier, S., Quintana Krupinski, N., Riedinger, N., Slomp, C., Snowball, I., Stepanova, A., Strano, S., Torti, A., Warnock, J., Xiao, N., and Zhang, R., 2015a. Methods. *In* Andrén, T., Jørgensen, B.B., Cotterill, C., Green, S., and the Expedition 347 Scientists, *Proc. IODP,* 347: College Station, TX (Integrated Ocean Drilling Program). **doi:10.2204/iodp.proc.347.102.2015**

Andrén, T., Jørgensen, B.B., Cotterill, C., Green, S., Andrén, E., Ash, J., Bauersachs, T., Cragg, B., Fanget, A.-S., Fehr, A., Granoszewski, W., Groeneveld, J., Hardisty, D., Herrero-Bervera, E., Hyttinen, O., Jensen, J.B., Johnson, S., Kenzler, M., Kotilainen, A., Kotthoff, U., Marshall, I.P.G., Martin, E., Obrochta, S., Passchier, S., Quintana Krupinski, N., Riedinger, N., Slomp, C., Snowball, I., Stepanova, A., Strano, S., Torti, A., Warnock, J., Xiao, N., and Zhang, R., 2015b. Site M0061. *In* Andrén, T., Jørgensen, B.B., Cotterill, C., Green, S., and the Expedition 347 Scientists, *Proc. IODP,* 347: College Station, TX (Integrated Ocean Drilling Program). **doi:10.2204/iodp.proc.347.105.2015**

Antonsson, K., Brooks, S.J., Seppä, H., Telford, R.J., and Birks, H.J.B., 2006. Quantitative palaeotemperature records inferred from fossil pollen and chironomid assemblages from Lake Gilltjärnen, northern central Sweden. *J. Quat. Sci.,* 21(8):831–841. **doi:10.1002/jqs.1004**

Hajdu, S., Larsson, U., and Skärlund, K., 1997. Växtplankton. *In* Elmgren, R., and Larsson, U. (Eds.), *Himmerfjärden: förändringar i ett näringsbelastat kustekosystem iÖstersjön (*Rapport 4565): Stockholm (Naturvårdsverketförlag), 63–79. (in Swedish, with abstract in English)

Hasle, G.R., and Syvertsen, E.E., 1990. Arctic diatoms in the Oslofjord and the Baltic Sea—a bio- and palaeogeographic problem. *In* Simmola, H. (Ed.), *Proceedings of the 10th International Diatom Symposium*: Koenigstein, Germany (Koeltz Scientific Books), 285–300.

Leventer, A., 1992. Modern distribution of diatoms in sediments from the George V Coast, Antarctica. *Mar. Micropaleontol.,* 19(4):315–332. **doi:10.1016/0377-8398(92)90036-J**

Snoeijs, P., Vilbaste, S., Potapova, M., Kasperoviciene, J., and Balashova, J. (Eds.), 1993–1998. *Intercalibration and Distribution of Diatom Species in the Baltic Sea* (Vol. 1–5): Uppsala, Sweden (Opulus Press).

Snowball, I.F., 1997. Gyroremanent magnetization and the magnetic properties of greigite-bearing clays in southern Sweden. *Geophys. J. Int.,* 129(3):624–636. **doi:10.1111/j.1365-246X.1997.tb04498.x**

Wallin, J.-E., 1996. History of sedentary farming in Ångermanland, northern Sweden, during the Iron Age and Medieval period based on pollen analytical investigations. *Veg. Hist. Archaeobot.,* 5(4):301–312. **doi:10.1007/BF00195298**

Weckström, K., and Juggins, S., 2006. Coastal diatom–environment relationships from the Gulf of Finland, Baltic Sea. *J. Phycol.,* 42(1):21–35. **doi:10.1111/j.1529-8817.2006.00166.x**

Publication: 20 February 2015
MS 347-106

Figure F1. Graphic lithology log summary log from a composite of Holes M0062A and M0062B.

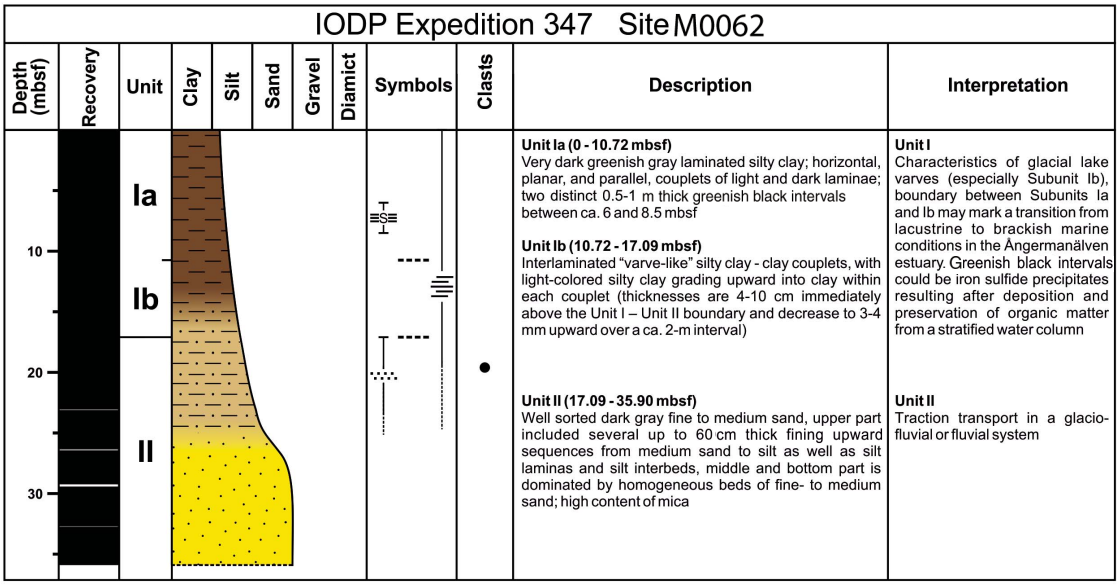

Figure F2. Rhythmites interpreted as varves (Sections 347-M0062D-5H-1 and 5H-2, 112–137 cm). Varve thickness changes from 20–40 mm in Section 5H-2 (right) to 3–4 mm in Section 5H-1 (left).

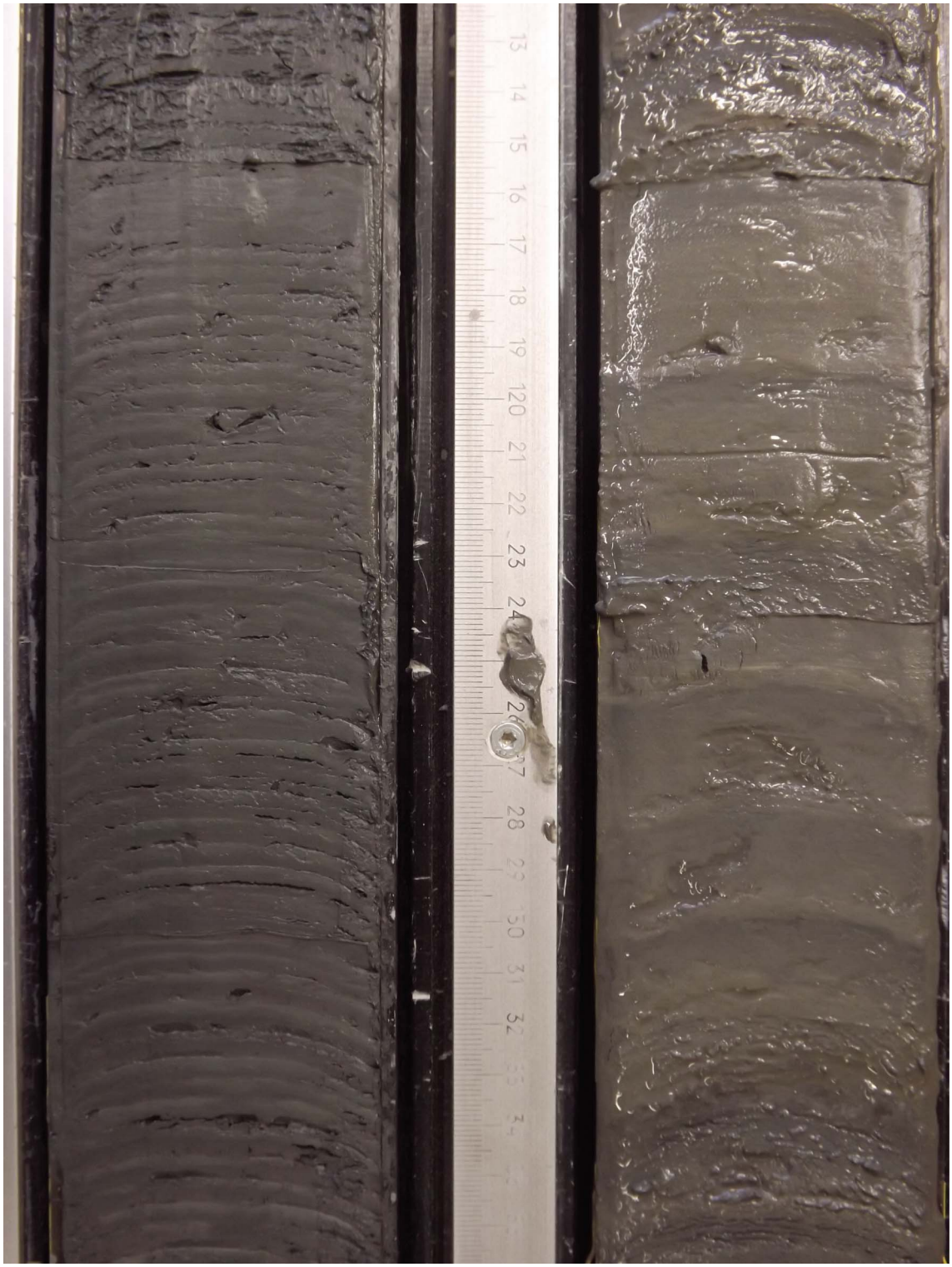

Figure F3. Diatom taxa showing different salinity affinities, Hole M0062A. Relative proportions of freshwater, brackish-freshwater, brackish, and brackish-marine diatom species are shown. Presence of sea ice related taxa (red dots), as well as proportions of planktonic and periphytic taxa, are also presented. Data are only qualitative presence/absence data and should be interpreted conservatively until quantitative data are generated.

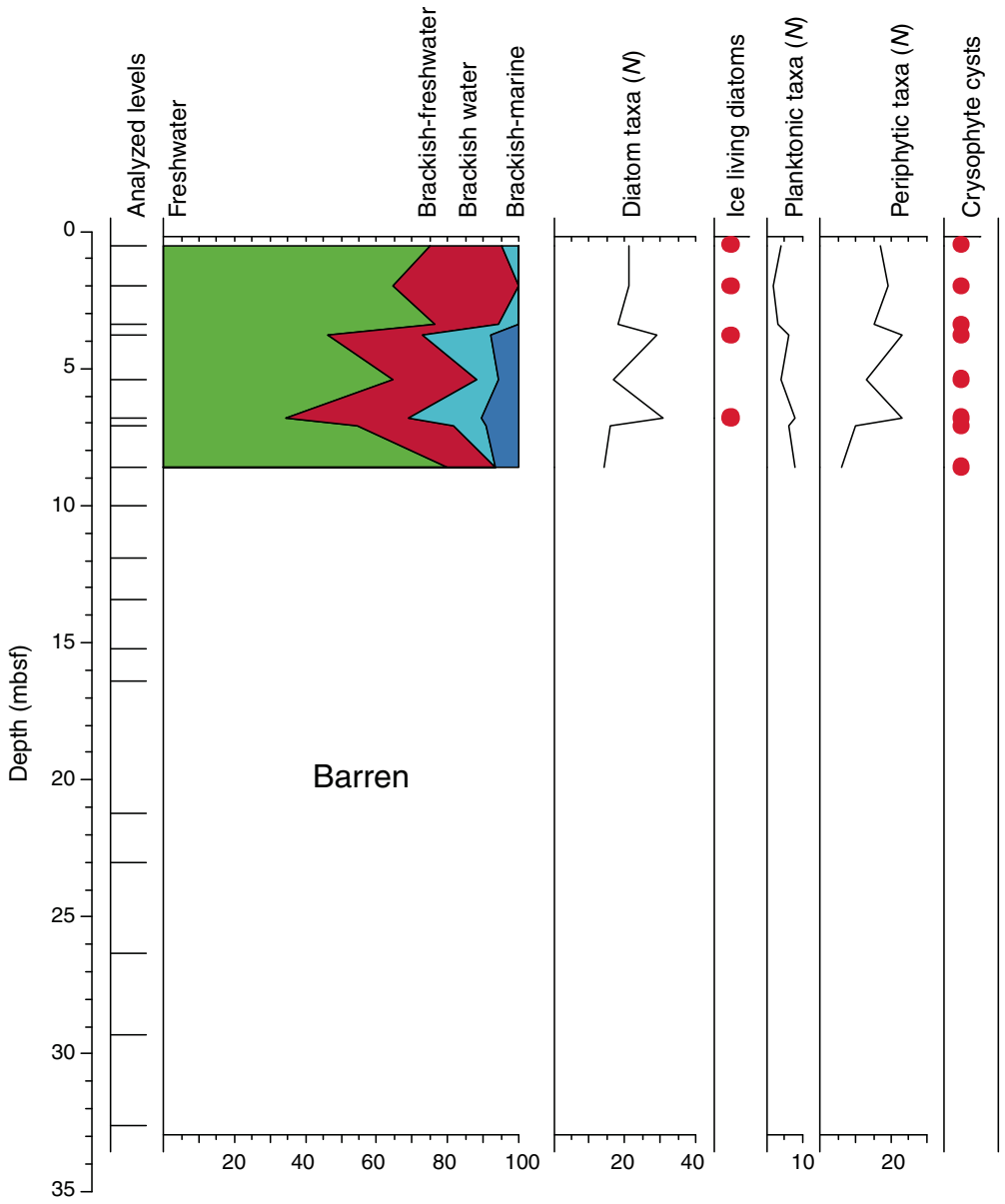

Figure F4. Palynomorphs, Hole M0062B. **1–3.** Pollen grains, (1) *Fraxinus* (ash, Core 347-M0062B-3H), (2) *Juniperus* (Core 347-M0062B-2H), (3) Cyperacea (sedge, Core 347-M0062B-2H). **4.** *Cosmarium* (freshwater alga, Core 347-M0062B-4H). **5.** Tintinnid (ciliate, Core 347-M0062B-2H). **6.** Insect jaw (*Corynoneura*?, Core 347-M0062B-3H). Scale bars = 20 µm.

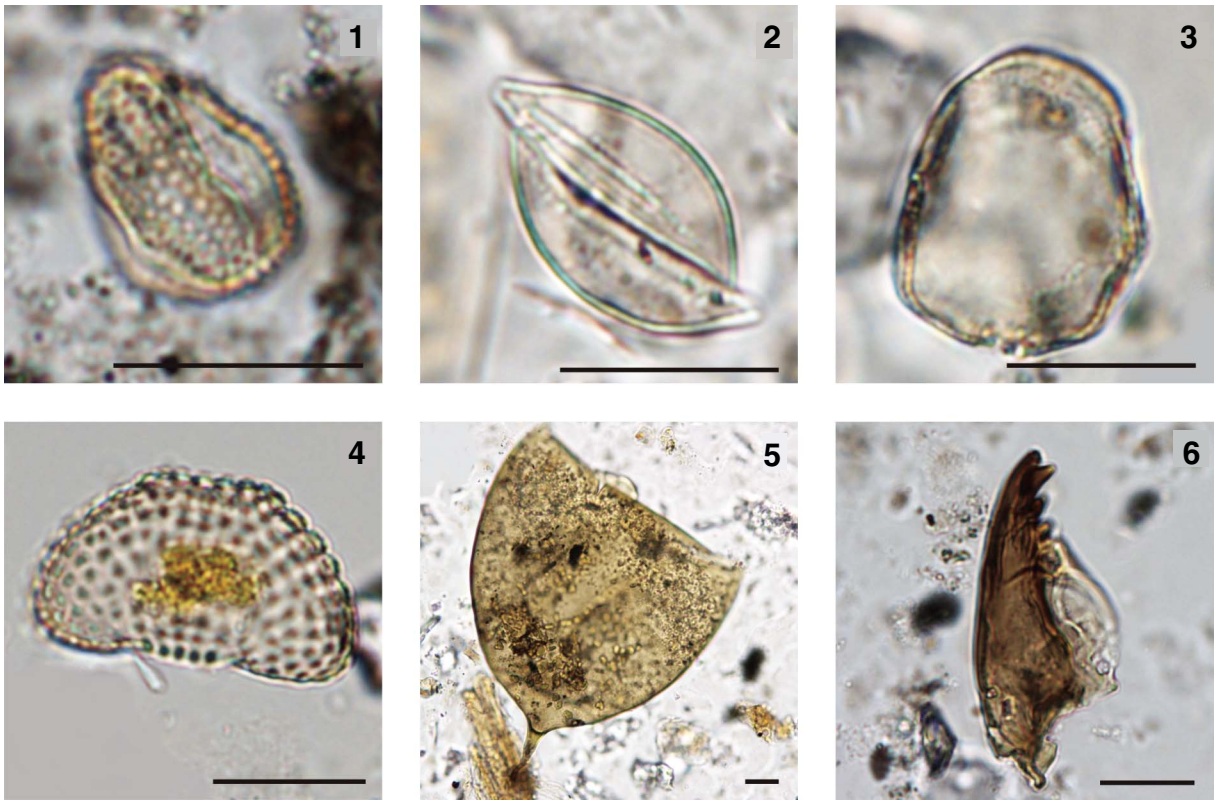

Figure F5. Pollen diagram with bisaccate pollen included in the reference sum, Site M0062. Data are mainly based on samples from Hole M0062B. Two samples from Hole M0062A (4.22 and 7.45 mbsf) were included. For all samples, between 100 and 210 pollen grains have been counted. Samples deeper than 14.27 mbsf in Hole M0062A and 14.35 mbsf in Hole M0062B were virtually barren of palynomorphs; these samples are not depicted here.

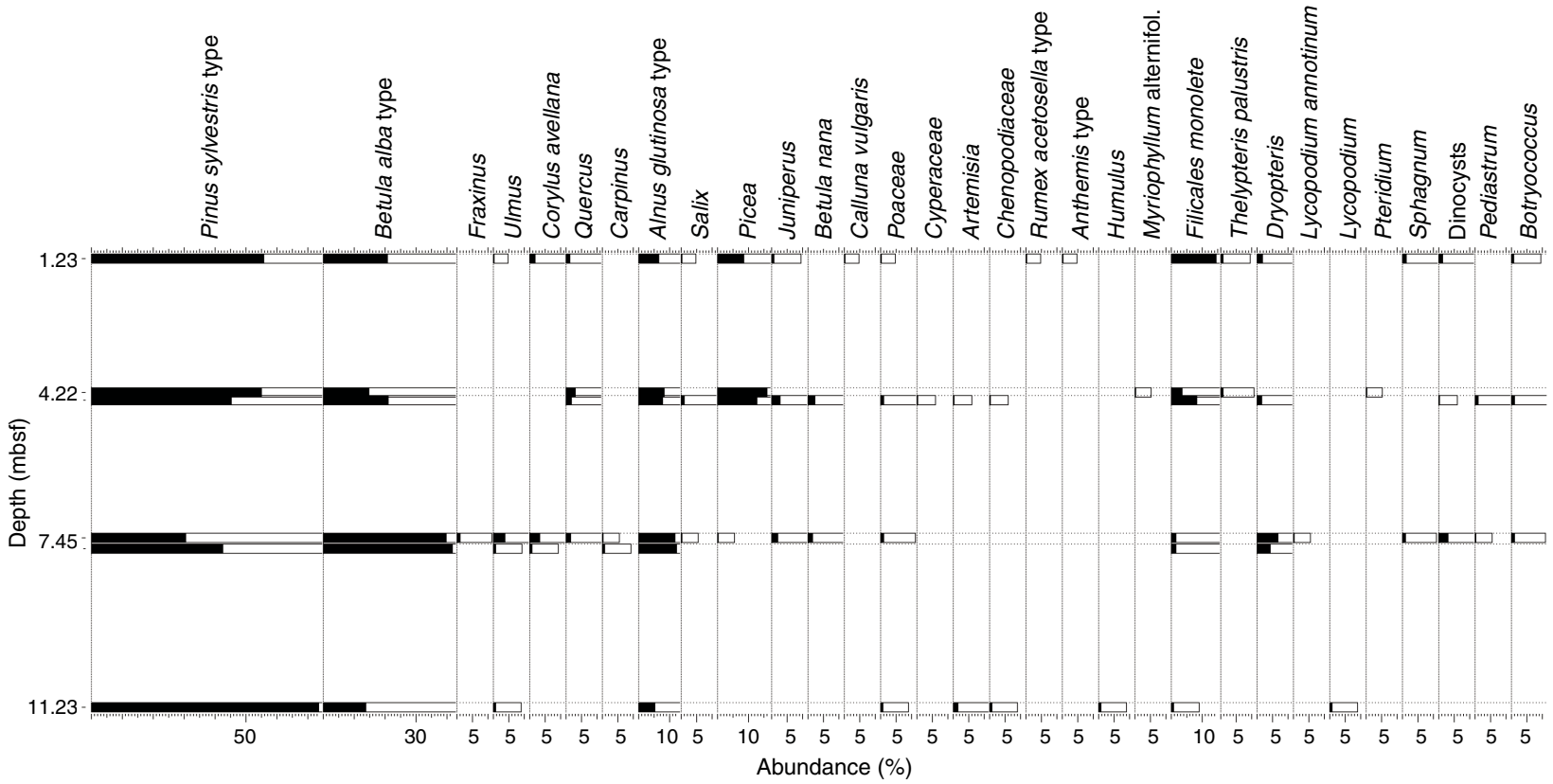

Figure F6. Simplified pollen diagram with main pollen types and palynomorph data, Hole M0062B. Includes two interjected samples from Hole M0062A (4.22 and 7.45 mbsf).

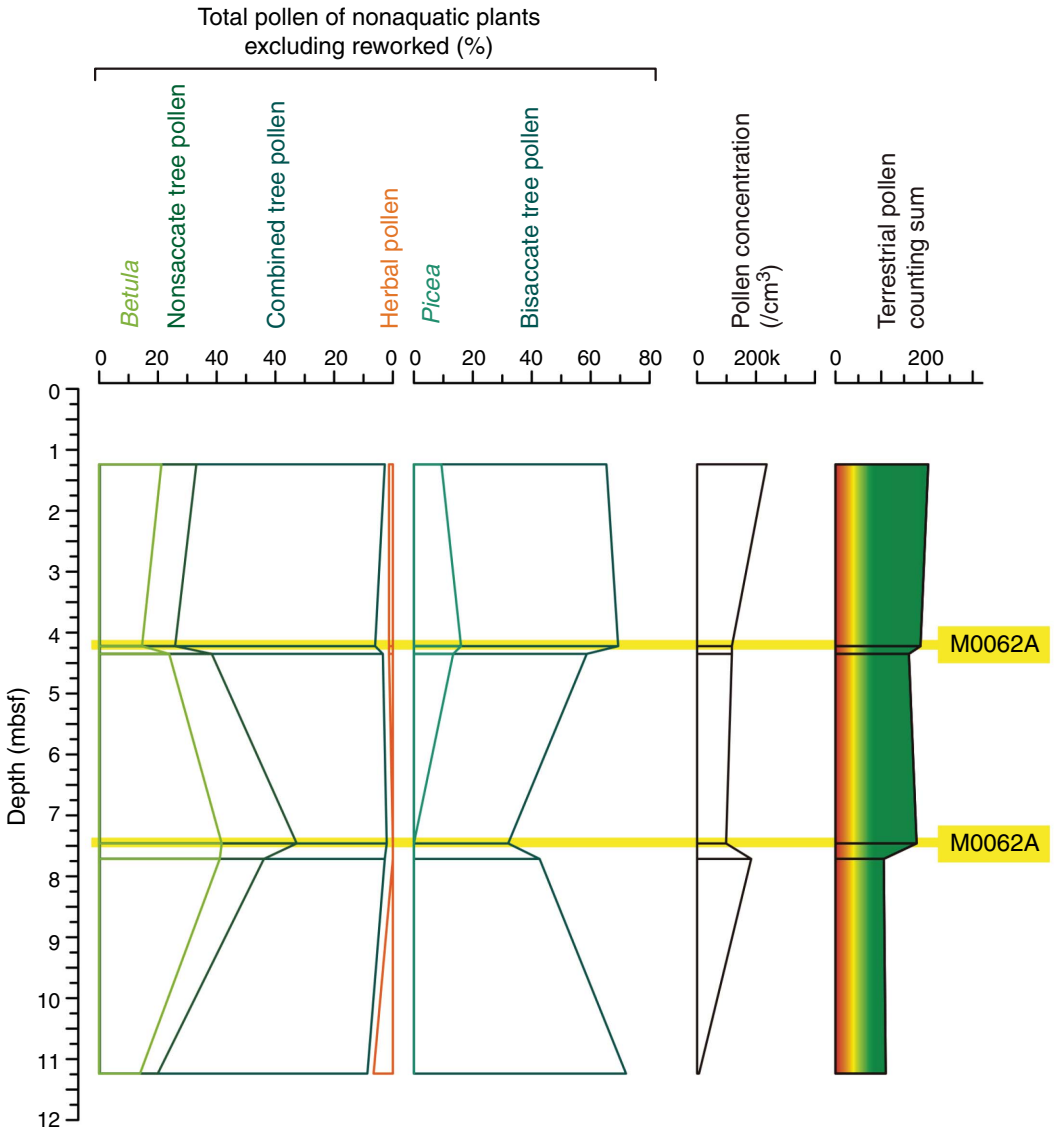

Figure F7. Concentrations of (**A**) chloride, (**B**) chloride-based salinity, (**C**) salinity by refractometer, and (**D**) alkalinity in interstitial water samples, Site M0062.

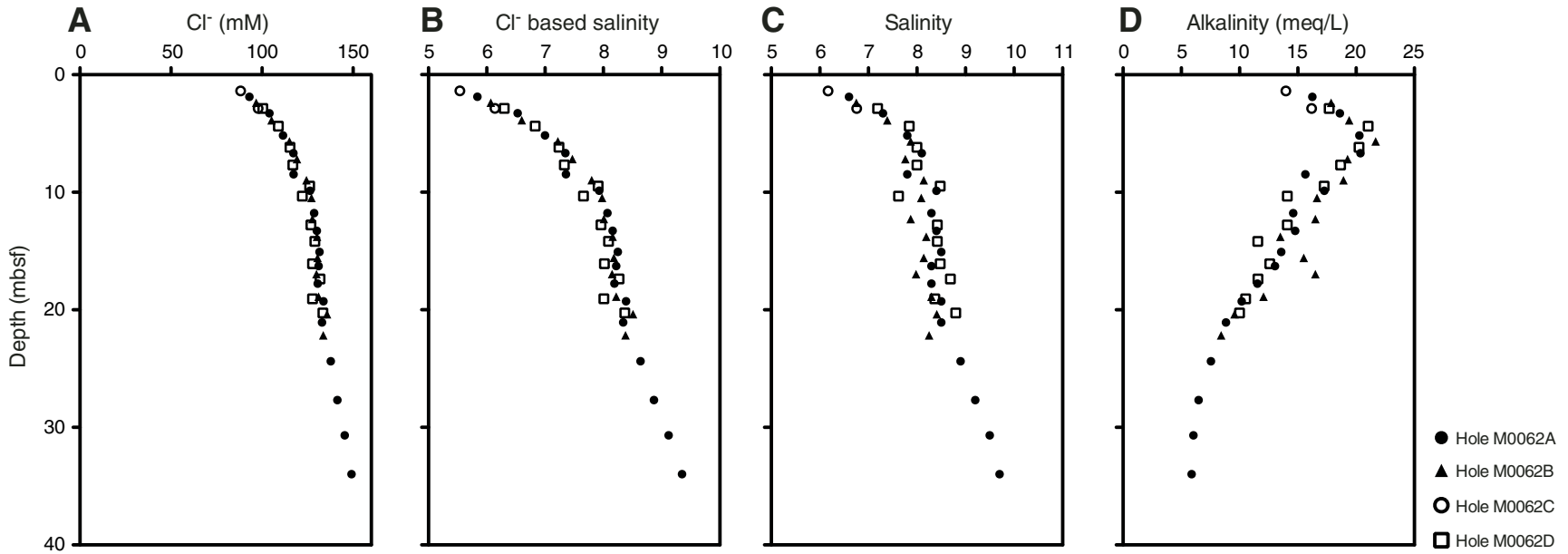

Figure F8. Concentrations of (A) sulfate, (B) sulfide, (C) ammonium, (D) phosphate, (E) iron, (F) manganese, and (G) pH from interstitial water samples, Site M0062.

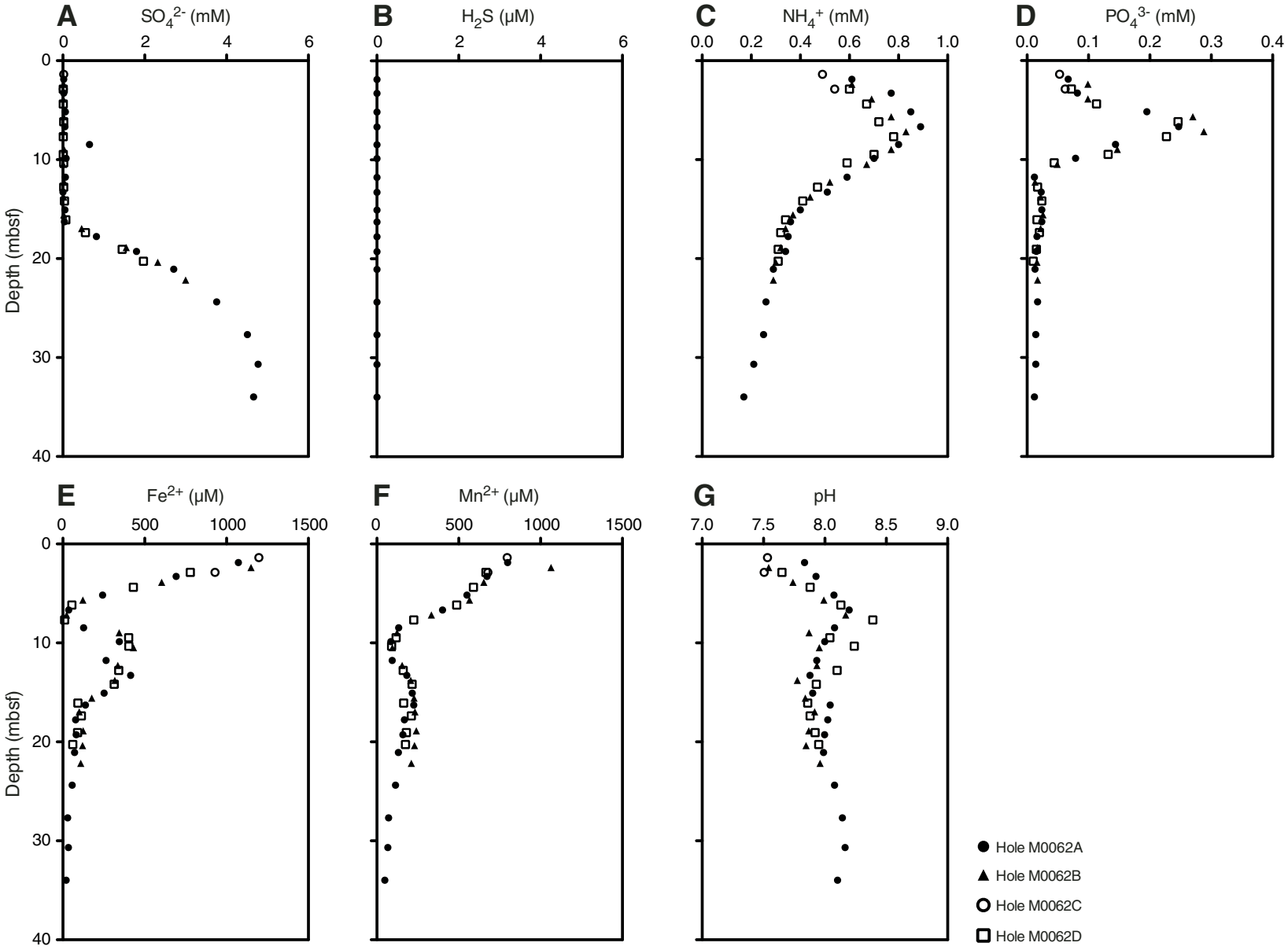

Figure F9. Concentrations and ratios of (**A**) bromide, (**B**) bromide/chloride, (**C**) boron, and (**D**) boron/chloride from interstitial water samples, Site M0062. Dashed lines = seawater ratio.

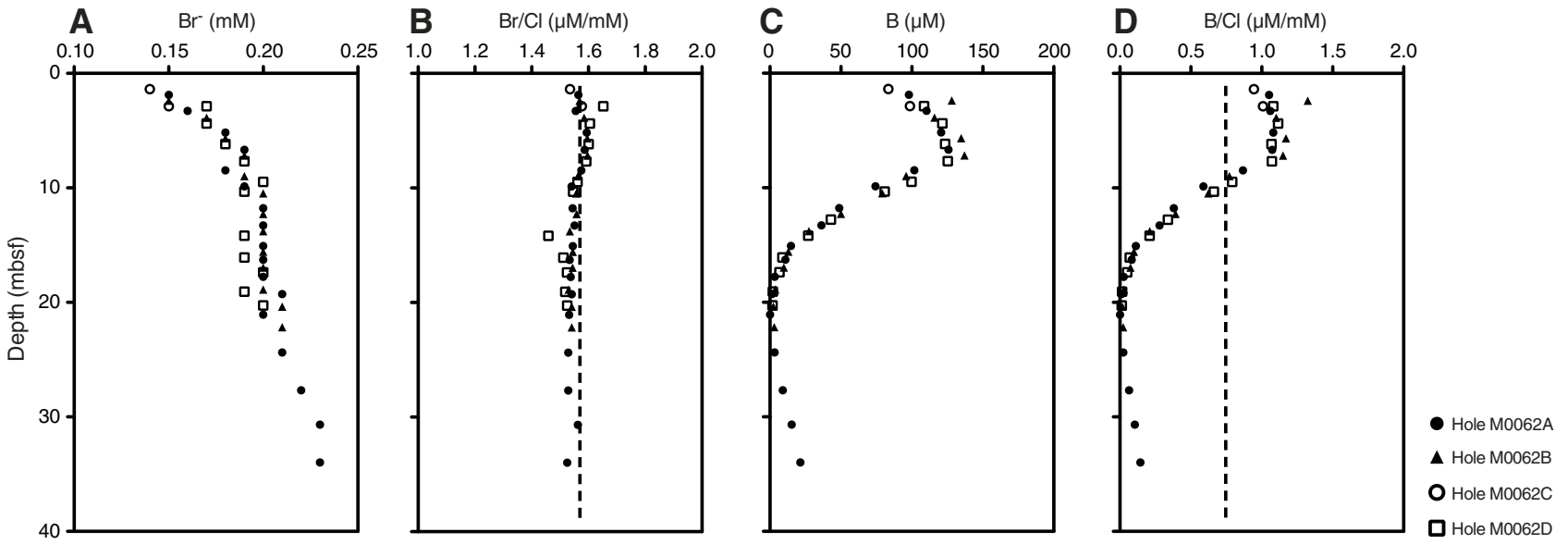

Figure F10. Concentrations and ratios of (**A**) sodium, (**B**) potassium, (**C**) magnesium, (**D**) calcium, (**E**) sodium/chloride, (**F**) potassium/chloride, (**G**) magnesium/chloride, and (**H**) calcium/chloride in interstitial water samples, Site M0062. Dashed lines = seawater ratio.

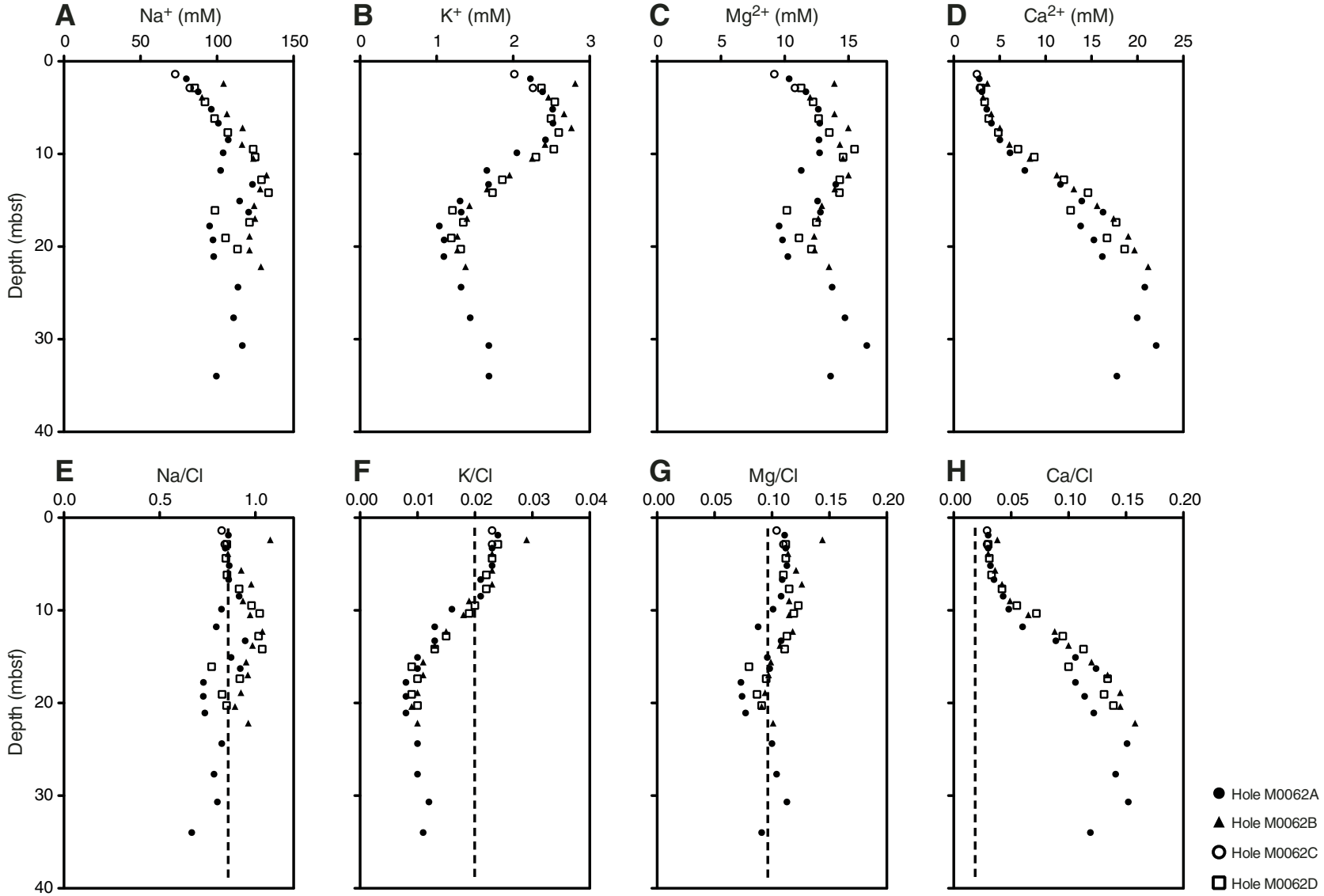

Figure F11. Concentrations of (**A**) strontium, (**B**) lithium, (**C**) barium, and (**D**) dissolved silica from interstitial water samples, Site M0062.

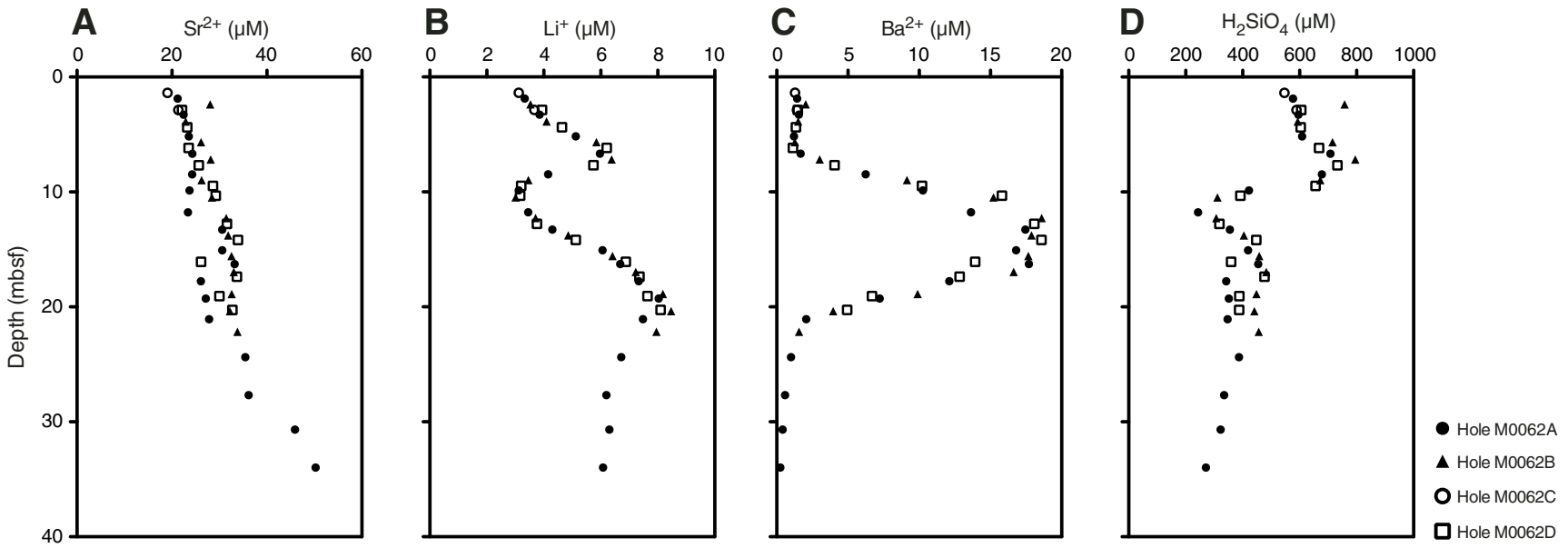

Figure F12. Solid phase concentrations of (**A**) total carbon (TC), (**B**) total organic carbon (TOC), (**C**) total inorganic carbon (TIC), and (**D**) total sulfur (TS), Site M0062.

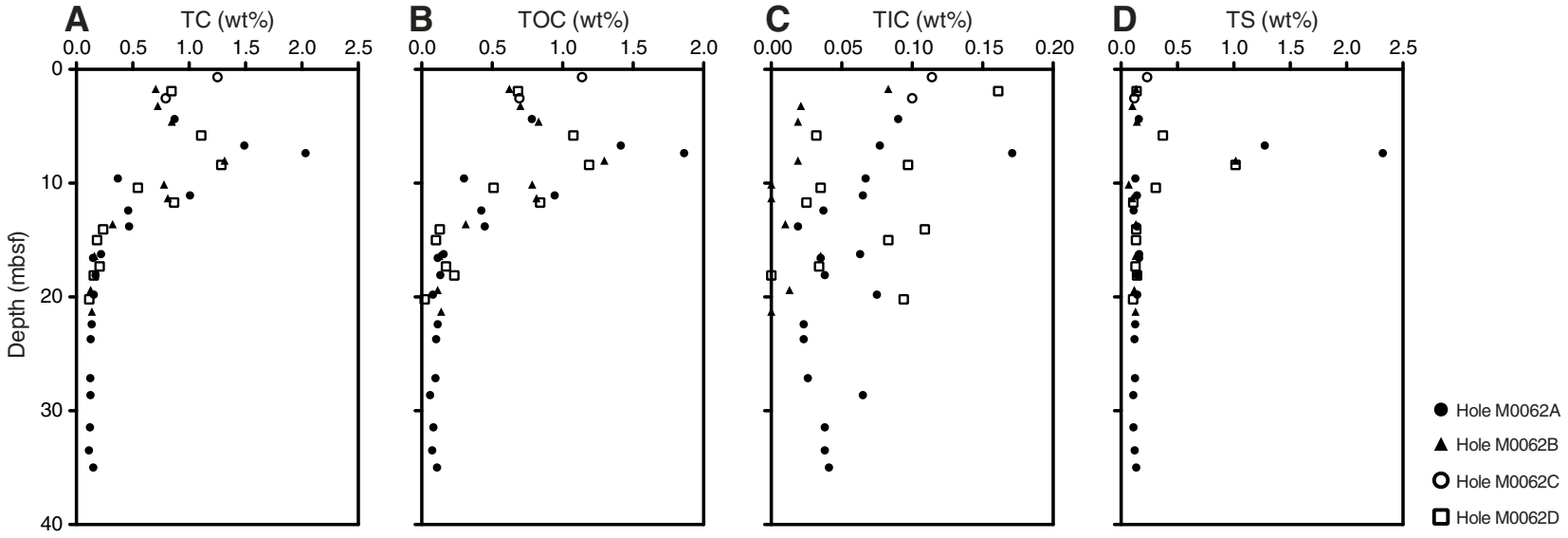

Figure F13. Natural gamma radiation (NGR) (cps), dry density (g/cm^3), MSCL-measured magnetic susceptibility (MS) (10^{-5} SI), color reflectance b*, and MSCL-measured *P*-wave velocity (m/s) in Hole M0062A.

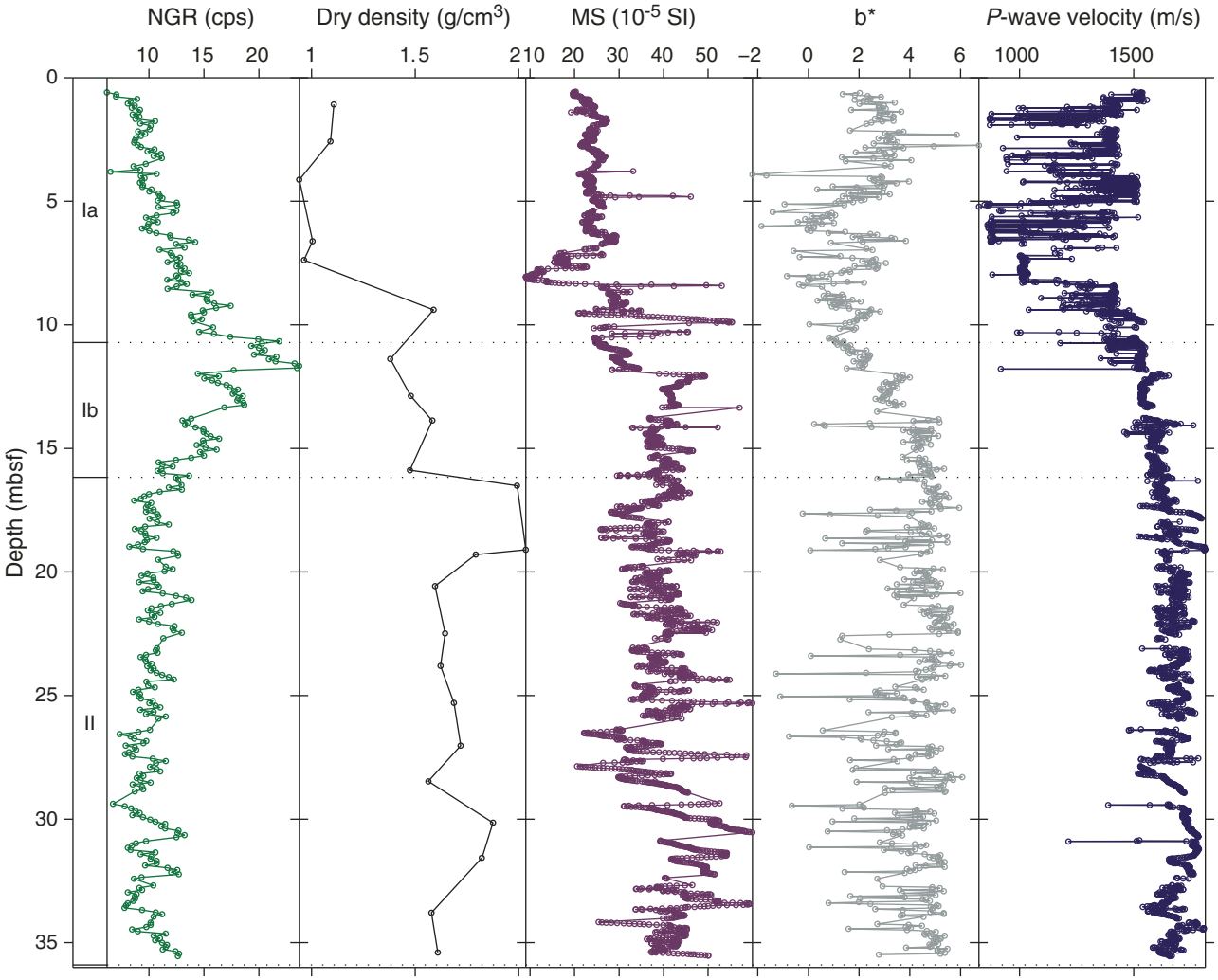

Figure F14. Gamma density (g/cm^3) and discrete bulk density (g/cm^3) measurements derived from pycnometer moisture and density analyses in Hole M0062A.

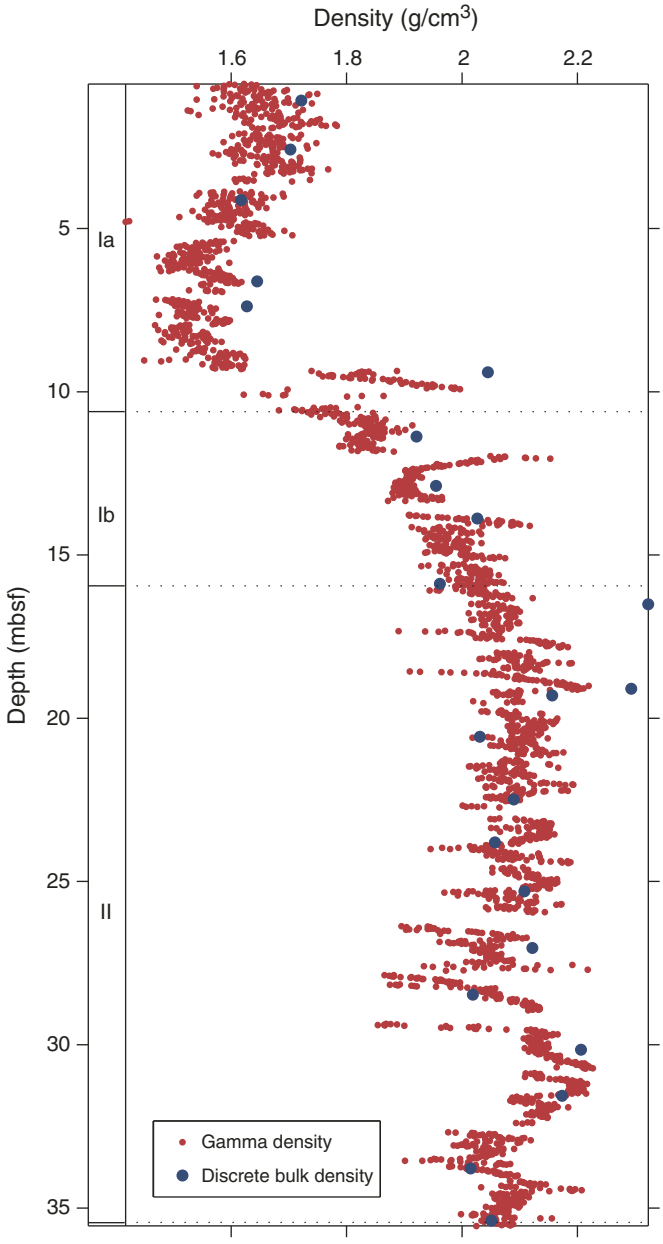

Figure F15. Correlation between gamma density (g/cm^3) and discrete bulk density (g/cm^3) measurements in Hole M0062A.

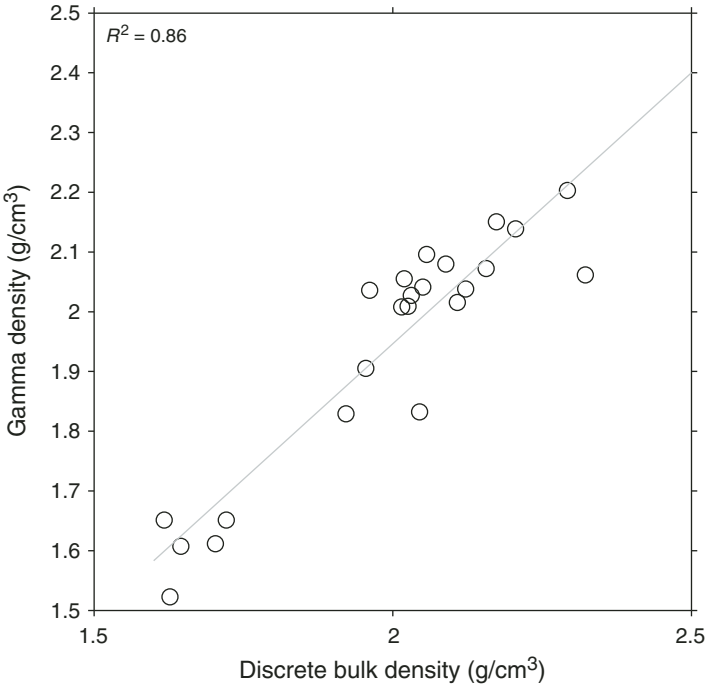

Figure F16. Plots and biplots of magnetic susceptibility (χ), natural remanent magnetization (NRM) intensity, and NRM inclination of discrete paleomagnetic samples, Holes M0062A, M0062C, and M0062D. Dashed line = geocentric axial dipole (GAD) prediction of inclination for the site latitude. AF = alternating field.

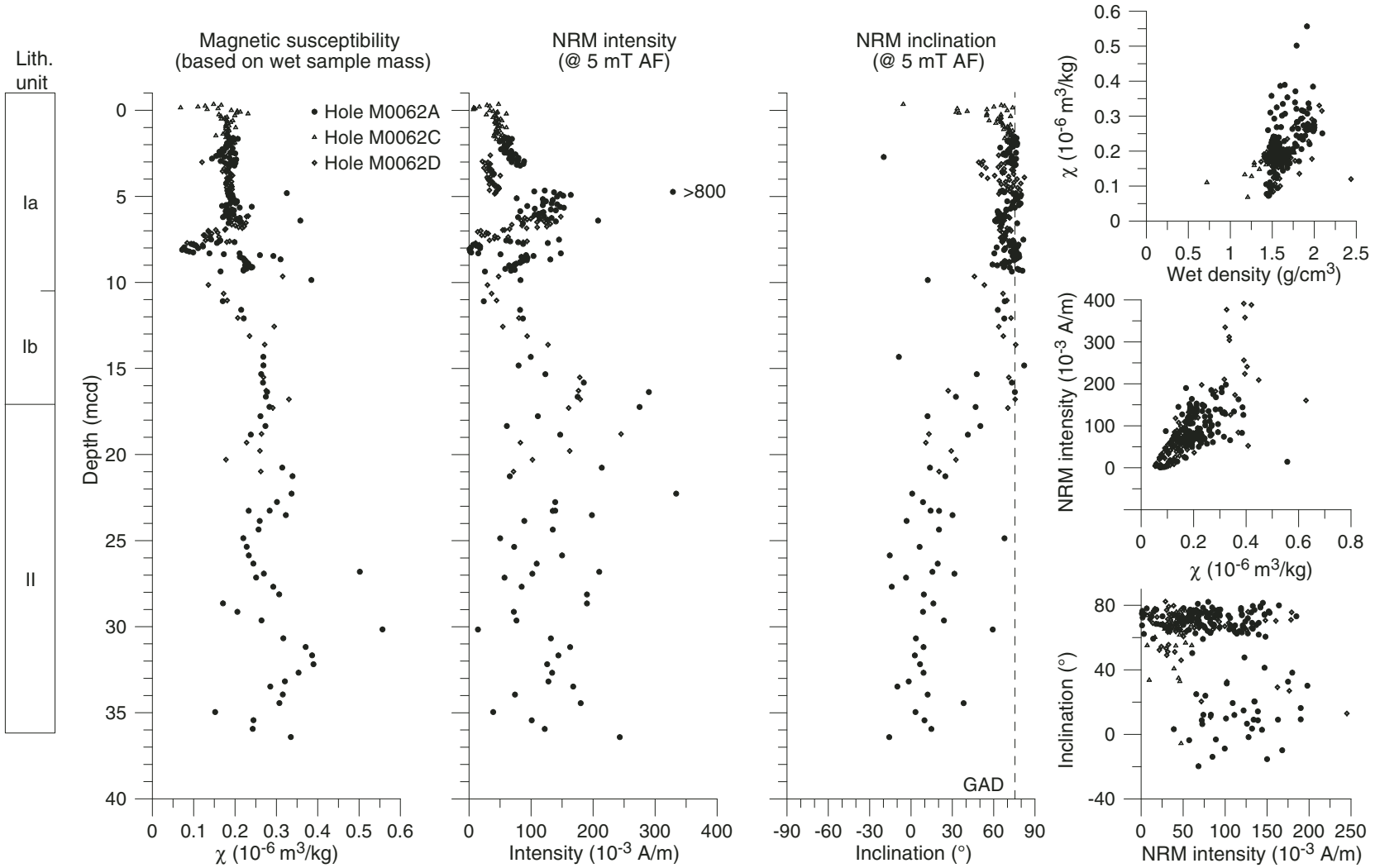

Figure F17. Plots of natural remanent magnetization (NRM) after alternating field (AF) demagnetization to 80 mT **A.** Sample 347-M0062A-6H-2, 105 cm; 16.64 mcd. **B.** Sample 347-M0062A-2H-2, 60 cm; 2.61 mcd. **C.** Sample 347-M0062-A-10H-1, 10 cm; 27.44 mcd. Categories 1 and 3 contain a vector that trends toward the origin during demagnetization, but it veers into a plane perpendicular to the last demagnetization axis, which is a sign of gyroremanent magnetization acquisition. The acquisition of GRM is most apparent in Category 3 (Sample 347-M0062A-6H-2, 105 cm). Category 2 contains a stable single-component NRM. Open squares = vertical, solid squares = horizontal.

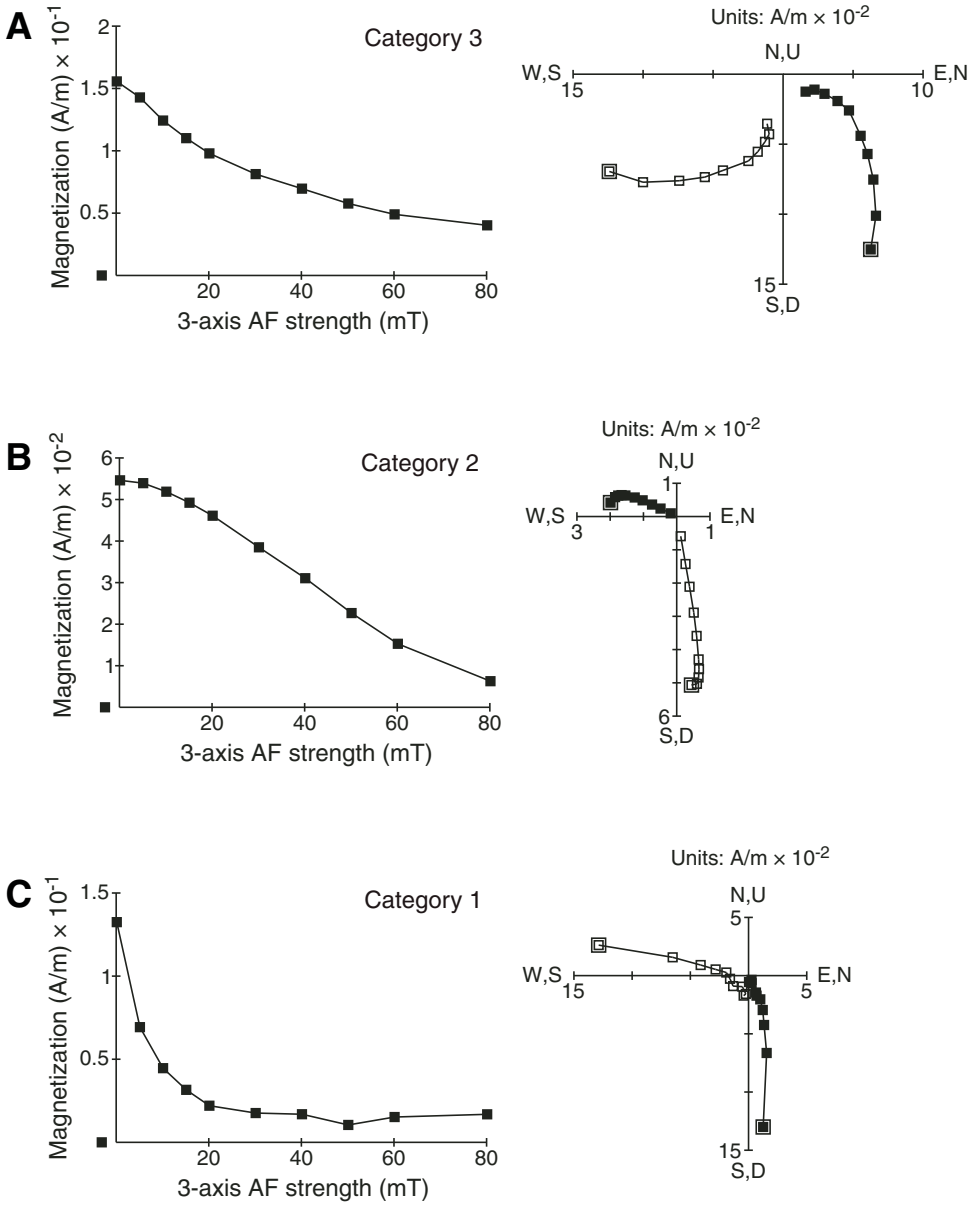

Figure F18. Plot of spliced magnetic susceptibility data, Site M0062.

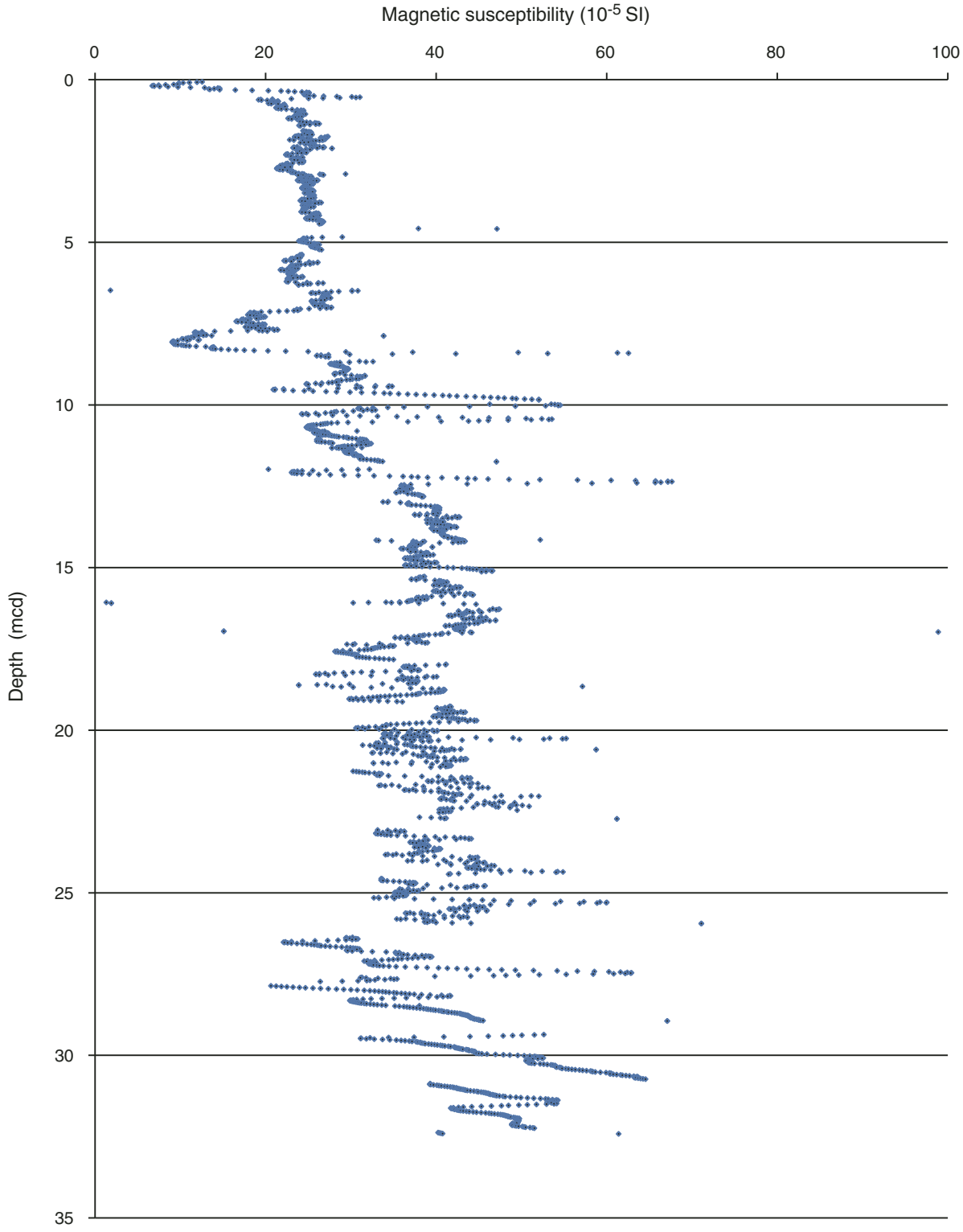

Figure F19. Correlation of seismic profile with lithologic boundaries and multisensor core logger magnetic susceptibility data (Hole M0062A), Site M0062. Units shown in figure are seismic Units I, II, and III that correspond to lithostratigraphic Subunits Ia and Ib and Unit II, respectively.

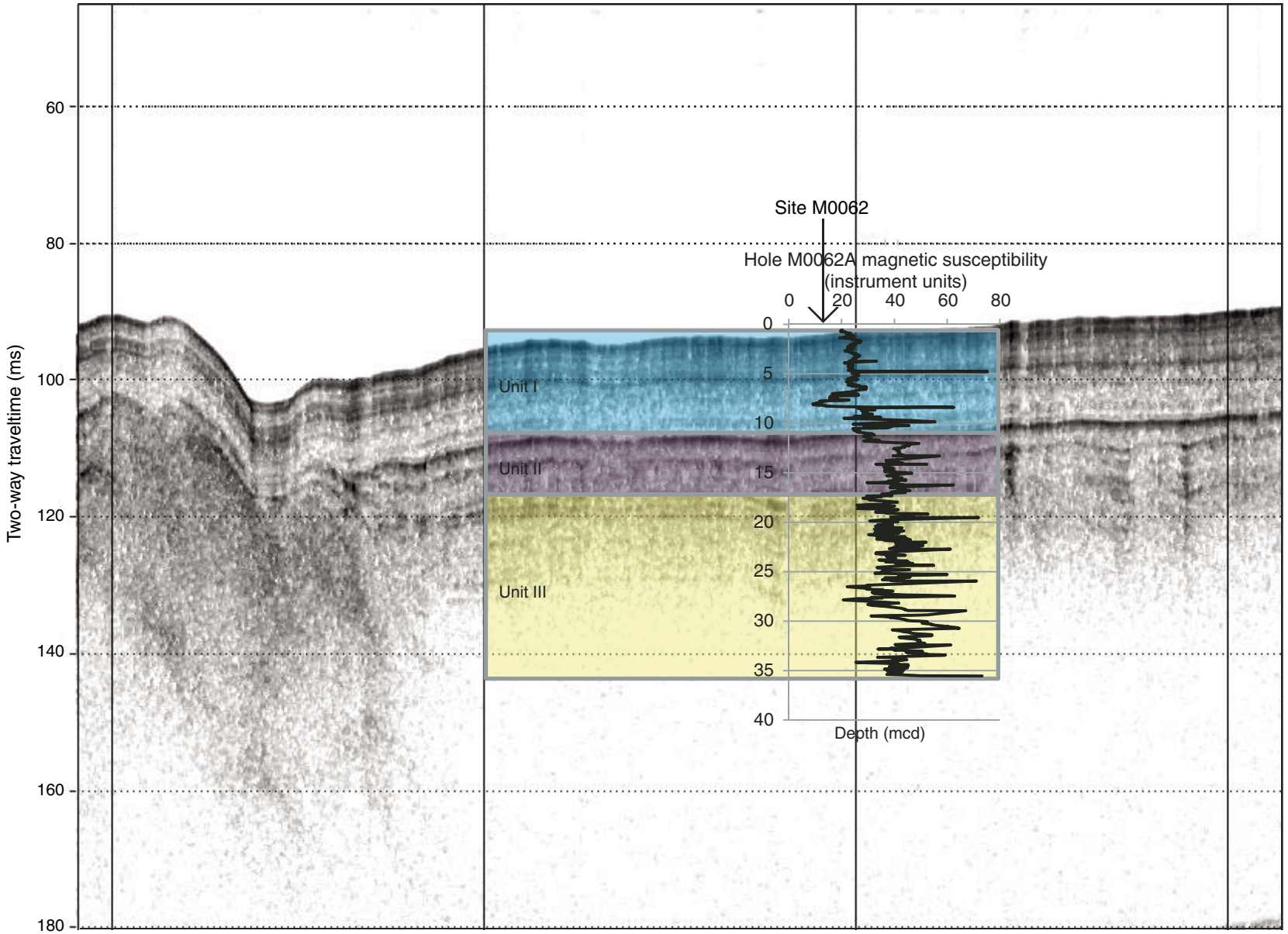

Figure F20. Gamma ray log, spectral gamma ray logs (K, U, and Th), and resistivity (red = deep induction, blue = medium, black = shallow) log, Hole M0062D. The drill pipe was set at 2 m WSF.

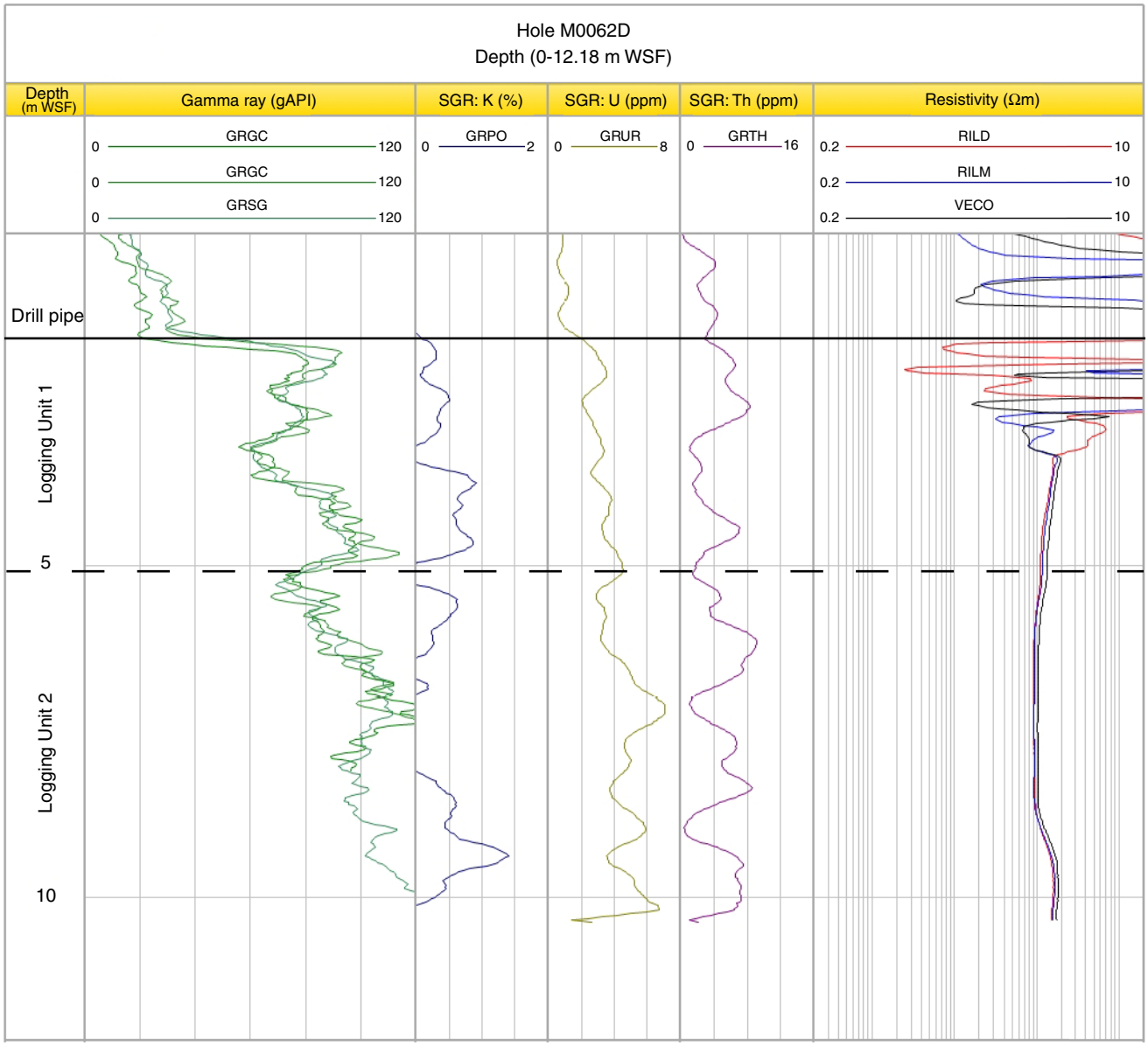

Table T1. Operations, Site M0062. (Continued on next page.)

Core	Coring method	Date (2013)	Time (UTC)	Depth (mbsf) Top	Depth (mbsf) Bottom	Recovered (m)	Recovery (%)	Mud type	Comments
347-M0062A-									
		5 Oct	1810						Arrived on site
		5 Oct	1830						Template down
		5 Oct	1910						Drill string down
		5 Oct	1930						Checked depth through clamps
1O	NCA	5 Oct	1940	0.00	0.50	0.00	0	Seawater	Washed down to avoid potential seabed contamination
2H	PCS	5 Oct	1946	0.50	3.80	3.36	101.82	Seawater	75 bar
3H	PCS	5 Oct	2022	3.80	7.10	3.40	103.03	Seawater	65 bar
4H	PCS	5 Oct	2054	7.10	10.40	3.41	103.33	Seawater	75 bar
5H	PCS	5 Oct	2140	10.40	13.70	3.36	101.82	Seawater	
6H	PCS	5 Oct	2230	13.70	16.40	2.81	104.07	Seawater	Difficulty in pulling back overshot, suspect due to sand
7H	PCS	5 Oct	2303	16.40	19.70	3.29	99.7	Guar	
8H	PCS	5 Oct	2340	19.70	23.00	3.19	96.67	Guar	
9H	PCS	6 Oct	0022	23.00	26.30	3.16	95.76	Guar	
10H	PCS	6 Oct	0057	26.30	29.30	2.73	91	Guar	
11H	PCS	6 Oct	0130	29.30	32.60	3.21	97.27	Guar	
12S	HS	6 Oct	0215	32.60	32.60	0.00	0	Guar	15 blows, no recovery save a few sand grains
13H	PCS	6 Oct	0238	32.60	35.90	3.15	95.45	Guar	No apparent fire pressure, 150 bar, down to 100, then back up; this repeated a couple of times before falling to zero without moving the pipe; full core recovered mainly sand with a small amount of silty clay at top
		6 Oct	0310						Called end of borehole as back in sand and clay
		6 Oct	0315						Started to prepare to trip the pipe
		6 Oct	0334						Seabed template off the seabed, moved to Hole M0062B
347-M0062B-									
		6 Oct	0423						Arrived on site
1O	NCA	6 Oct	0438	0.00	1.00	0.00	0	Seawater	
2H	PCS	6 Oct	0445	1.00	4.30	3.49	105.76	Seawater	Smooth firing and pressure reduction
3H	PCS	6 Oct	0515	4.30	7.60	3.46	104.85	Seawater	Smooth firing and pressure reduction
4H	PCS	6 Oct	0545	7.60	10.90	3.48	105.45	Seawater	Smooth firing and pressure reduction but not to zero initially
5H	PCS	6 Oct	0610	10.90	14.20	3.21	97.27	Seawater	Fired and dropped pressure, then rose to 135 bar and stopped before clearing when pipe lifted; good core but silt at base; changed overshot pins
		6 Oct	0650						Did not pressure up; retrieved to inspect; all intact and seals fine; pumped mud into the hole before retrying
6H	PCS	6 Oct	0710	14.20	17.50	3.21	97.27	Seawater	Smooth firing and pressure drop; required two attempts to pull corer out of BHA; good core; no shoe sample
7H	PCS	6 Oct	0750	17.50	20.80	3.25	98.48	Seawater	Smooth firing but erratic pressure reduction
8H	PCS	6 Oct	0815	20.80	24.10	3.20	96.97	Seawater	Good silty core.
		6 Oct	0825						End of hole
		6 Oct	0840						Tripping pipe
		6 Oct	0900						Bumped over to next location
347-M0062C-									
		6 Oct	0900						Arrived on site
		6 Oct	0920						Prepared to take sample from seabed down without seabed template on seafloor
1H	PCS	6 Oct	0930	0.00	3.30	3.43	103.94	Seawater	Fired at 80 bar and down to zero; full stroke
347-M0062D-									
		6 Oct	1000						Arrived on site
1O	NCA	6 Oct	1025	0.00	1.50	0.00	0	Seawater	Washed down to create core run offset for composite splice
2H	PCS	6 Oct	1035	1.50	4.80	3.45	104.55	Seawater	Smooth firing and pressure reduction
3H	PCS	6 Oct	1105	4.80	8.10	3.43	103.94	Seawater	55 bar, smooth firing and pressure reduction
4H	PCS	6 Oct	1145	8.10	11.40	3.41	103.33	Seawater	34 bar only
5H	PCS	6 Oct	1220	11.40	14.70	3.47	105.15	Seawater	
6H	PCS	6 Oct	1255	14.70	17.70	3.00	100	Guar	

Table T1 (continued).

Core	Coring method	Date (2013)	Time (UTC)	Depth (mbsf) Top	Depth (mbsf) Bottom	Recovered (m)	Recovery (%)	Mud type	Comments
		6 Oct	1335					Guar	Pressure up to 220 bar with no lowering until release valve opened; on recovery found that piston had not fired and seal had been lost; recovered to deck and serviced
7H	PCS	6 Oct	1405	17.70	21.00	3.30	100	Guar	Pressure wavered around 75 bar and dropped right back to zero
		6 Oct	1425						End of hole
		6 Oct	1425						Washed out remainder of API pipe to form rathole for logging
		6 Oct	1440						Tripped pipe to 1.5 mbsf
		6 Oct	1640						Logging: 2 runs before hole closed at 7 mbsf

HS = hammer sampler, NCA = noncoring assembly, PCS = piston coring system. BHA = bottom-hole assembly, API = American Petroleum Institute size drill pipe.

Table T2. Diatom species, Site M0062.

Taxonomic list
Brackish-marine taxa
Achnanthes brevipes var. *intermedia* (Kützing) Cleve
Chaetoceros spp. resting spores
Chaetoceros spp. vegetative cells
Hantzschia virgata var. *gracilis* Hustedt in Schmidt
Stauroneis cf. *radissonii* (Poulin and Cardinal)
Tabularia waernii Snoeijs
Brackish taxa
Achnanthes lemmermannii Hustedt
Amphora robusta Gregory
Brachysira aponina Kützing
Cocconeis scutellum Ehrenberg
Cyclotella choctawhatcheeana Prasad
Mastogloia pusilla Grunow
Melosira moniliformis (Müller) Agardh
Nitzschia cf. *angustulata* Krammer and Lange-Bertalot
Pinnularia halophila Krammer
Rhoicosphenia curvata (Kützing) Grunow
Thalassiosira levanderi Van Goor
Pauliella taeniata (Grunow) Round and Basson
Tabularia cf. *laevis* Kützing
Brackish-freshwater taxa
Fragilariopsis cylindrus (Grunow) Krieger
Achnanthidium microcephalum Kützing
Cocconeis pediculus Ehrenberg
Cocconeis placentula Ehrenberg
Ctenophora pulchella (Ralfs ex Kützing) Williams and Round
Cyclotella meneghiniana Kützing
Diatoma vulgaris de Saint-Vincent
Diploneis smithii (Brébisson)
Epithemia sorex Kützing
Gomphonema olivaceum (Hornemann) Kützing
Gomphonema parvulum Grunow
Mastogloia baltica Grunow in van Huerck
Melosira lineata (Dillwyn) C.A. Agardh
Navicula capitata Ehrenberg
Navicula cincta (Ehrenberg) Ralfs
Navicula rhynchocephala Kützing
Nitzschia frustulum (Kützing) Grunow
Rhopalodia gibba (Ehrenberg) Müller
Surirella brebissonii Krammer and Lange-Bertalot
Tabularia tabulata (C.A. Agard) Snoeijs
Freshwater taxa
Achnanthes subatomides (Hustedt) Lange-Bertalot and Archibald
Amphora copulata (Kützing) Schoeman and Archibald
Aulacoseira alpigena (Grunow) Krammer
Aulacoseira ambigua (Grunow) Simonsen
Aulacoseira islandica (Müller) Simonsen
Aulacoseira subarctica (Müller) Haworth
Brachysira vitrea (Grunow) Ross
Caloneis cf. *silicula* Ehrenberg
Cocconeis disculus (Schumann) Cleve
Cyclotella atomus Hustedt
Cyclotella ocellata Pantocsek
Cyclotella radiosa (Grunow) Lemmermann
Cyclotella rossii Håkansson
Cyclotella schumannii (Grunow) Håkansson
Cyclotella stelligera Cleve and Grunow
Cymbella affinis Kützing
Cymbella angustata (W. Smith) Cleve
Diatoma tenuis Agardh
Diploneis parma Cleve
Encyonema minutum (Hilse) Mann
Encyonema silesiacum (Bleisch) Mann
Eucocconeis flexella (Kützing) Meister
Eunotia cf. *septentrionalis* Østrup
Eunotia implicata Nörpel, Lange-Bertalot and Alles
Eunotia triodon Ehrenberg
Fragilaria capucina Desmazières
Fragilaria capucina var. *gracilis* (Oestrup) Hustedt
Fragilaria tenera (Smith) Lange-Bertalot
Frustulia rhomboides var. *crassinervia* (Brébisson) Ross
Gomphocymbella ancyli (Cleve) Hustedt
Gomphonema acuminatum var. *coronatum* (Ehrenberg) Ehrenberg
Gomphonema angustum C. Agardh
Gomphonema clavatum Ehrenberg
Karayevia clevei (Grunow) Bukhiyarova
Navicula scutelloides Smith
Pinnularia subcapitata Gregory
Sellaphora pupula (Kützing) Mereschowsky
Stauroneis phoenicenteron (Nitzsch) Ehrenberg
Staurosira construens Ehrenberg
Staurosira venter (Ehrenberg) H. Kobayasi
Staurosirella lapponica (Grunow) Williams and Round
Staurosirella pinnata (Ehrenberg) Williams and Round
Stephanodiscus minutulus (Kützing) Round
Stephanodiscus neoastraea Håkansson and Hickel
Synedra ulna (Nitzsch) Ehrenberg
Tabelaria flocculosa (Roth) Kützing

Salinity affinities follows Snoeijs et al. (1993–1998). Diatom authorities according to AlgaeBase (**www.algaebase.org**).

Table T3. Diatoms, Hole M0062A. This table is available in an **oversized format.**

Table T4. Calculated salinity and elemental ratios of interstitial waters, Site M0062.

Core, section, interval (cm)	Type	Depth (mbsf)	Cl^- based salinity	Anion-based salinity	Na/Cl (mM/mM)	Ca/Cl (mM/mM)	Mg/Cl (mM/mM)	K/Cl (mM/mM)	Br/Cl (µM/mM)	B/Cl (µM/mM)
347-M0062A-										
2H-1, 135–140	Rh	1.88	5.84	7.71	0.86	0.03	0.11	0.02	1.56	1.05
2H-2, 125–130	Rh	3.28	6.53	9.80	0.84	0.03	0.11	0.02	1.56	1.06
3H-1, 135–140	Rh	5.18	7.00	12.17	0.86	0.03	0.11	0.02	1.59	1.08
3H-2, 135–140	Rh	6.68	7.35	14.03	0.86	0.04	0.11	0.02	1.59	1.07
4H-1, 135–140	Rh	8.48	7.36	15.84	0.91	0.04	0.11	0.02	1.57	0.87
4H-2, 125–130	Rh	9.88	7.93	17.80	0.82	0.05	0.10	0.02	1.54	0.59
5H-1, 135–140	Rh	11.78	8.07	19.84	0.80	0.06	0.09	0.01	1.54	0.38
5H-2, 135–140	Rh	13.28	8.16	21.43	0.95	0.09	0.11	0.01	1.55	0.28
6H-1, 135–140	Rh	15.08	8.25	23.33	0.87	0.11	0.10	0.01	1.54	0.11
6H-2, 106–111	Rh	16.29	8.22	24.50	0.92	0.12	0.10	0.01	1.53	0.08
7H-1, 135–140	Rh	17.78	8.19	25.97	0.73	0.11	0.07	0.01	1.54	0.03
7H-2, 135–140	Rh	19.28	8.39	27.66	0.73	0.11	0.07	0.01	1.54	0.01
8H-1, 135–140	Rh	21.08	8.34	29.41	0.74	0.12	0.08	0.01	1.53	—
9H-1, 135–140	Rh	24.38	8.64	33.02	0.82	0.15	0.10	0.01	1.53	0.02
10H-1, 135–140	Rh	27.68	8.87	36.54	0.78	0.14	0.10	0.01	1.53	0.06
11H-1, 135–140	Rh	30.68	9.12	39.79	0.80	0.15	0.11	0.01	1.56	0.10
13H-1, 135–140	Rh	33.98	9.35	43.33	0.67	0.12	0.09	0.01	1.53	0.14
347-M0062B-										
2H-1, 135–140	Rh	2.38	6.07	8.45	1.08	0.04	0.14	0.03	1.57	1.32
2H-2, 135–140	Rh	3.88	6.60	10.48	0.86	0.03	0.11	0.02	1.58	1.10
3H-1, 135–140	Rh	5.68	7.22	12.89	0.93	0.04	0.12	0.02	1.60	1.17
3H-2, 135–140	Rh	7.18	7.47	14.65	0.98	0.04	0.13	0.02	1.60	1.15
4H-1, 135–140	Rh	8.98	7.80	16.78	0.93	0.05	0.12	0.02	1.56	0.77
4H-2, 125–130	Rh	10.48	7.98	18.45	0.97	0.07	0.11	0.02	1.56	0.62
5H-1, 135–140	Rh	12.28	8.01	20.28	1.04	0.09	0.12	0.02	1.56	0.39
5H-2, 135–140	Rh	13.78	8.16	21.94	0.99	0.10	0.11	0.01	1.53	0.21
6H-1, 135–140	Rh	15.58	8.18	23.76	0.95	0.12	0.10	0.01	1.55	0.10
6H-2, 124–129	Rh	16.97	8.15	25.11	0.96	0.13	0.10	0.01	1.54	0.07
7H-1, 135–140	Rh	18.88	8.22	27.10	0.92	0.15	0.09	0.01	1.53	0.03
7H-2, 135–140	Rh	20.38	8.51	28.89	0.89	0.15	0.09	0.01	1.54	0.02
8H-1, 135–140	Rh	22.18	8.38	30.56	0.96	0.16	0.10	0.01	1.54	0.02
347-M0062C-										
1H-1, 135–140	Rh	1.38	5.54	6.91	0.82	0.03	0.10	0.02	1.54	0.95
1H-2, 135–140	Rh	2.88	6.14	9.01	0.84	0.03	0.11	0.02	1.58	1.01
347-M0062D-										
2H-1, 135–140	Rh	2.88	6.30	9.17	0.85	0.03	0.11	0.02	1.65	1.08
2H-2, 135–140	Rh	4.38	6.83	11.21	0.85	0.03	0.11	0.02	1.60	1.12
3H-1, 135–140	Rh	6.18	7.24	13.41	0.85	0.03	0.11	0.02	1.60	1.07
3H-2, 135–140	Rh	7.68	7.33	15.01	0.92	0.04	0.12	0.02	1.59	1.07
4H-1, 135–140	Rh	9.48	7.91	17.39	0.98	0.06	0.12	0.02	1.56	0.79
4H-2, 125–130	Rh	10.33	7.66	17.98	1.02	0.07	0.12	0.02	1.55	0.66
5H-1, 135–140	Rh	12.78	7.96	20.73	1.02	0.09	0.11	0.01	—	0.34
5H-2, 125–130	Rh	14.18	8.09	22.27	1.04	0.11	0.11	0.01	1.46	0.21
6H-1, 135–140	Rh	16.08	8.02	24.09	0.77	0.10	0.08	0.01	1.51	0.07
6H-2, 115–120	Rh	17.38	8.27	25.65	0.92	0.13	0.09	0.01	1.52	0.05
7H-1, 134–139	Rh	19.07	8.01	27.08	0.83	0.13	0.09	0.01	1.52	0.02
7H-2, 104–109	Rh	20.27	8.37	28.64	0.85	0.14	0.09	0.01	1.53	0.01

Rh = Rhizon sample. — = no data are reported for samples with insufficient pore water volumes.

Table T5. Interstitial water geochemistry, Site M0062. This table is available in an **oversized format.**

Table T6. Total carbon (TC), total organic carbon (TOC), total inorganic carbon (TIC), and total sulfur (TS) in sediment, Site M0062.

Core, section, interval (cm)	Depth (mbsf)	TC (wt%)	TOC (wt%)	TIC (wt%)	TS (wt%)
347-M0062A-					
3H-1, 55.5–57	4.36	0.87	0.78	0.09	0.16
3H-2, 138.5–140	6.69	1.49	1.41	0.08	1.28
4H-1, 26–27	7.36	2.03	1.86	0.17	2.32
4H-2, 98–99	9.58	0.37	0.30	0.07	0.13
5H-1, 67.5–69	11.08	1.01	0.94	0.07	0.14
5H-2, 50–52	12.40	0.46	0.42	0.04	0.11
6H-1, 9–10	13.79	0.47	0.45	0.02	0.14
6H-2, 103–104	16.23	0.22	0.15	0.06	0.16
7H-1, 17–18	16.57	0.15	0.11	0.03	0.16
7H-2, 17–18	18.07	0.17	0.13	0.04	0.14
8H-1, 10–12	19.80	0.15	0.08	0.08	0.14
8H-2, 120–121	22.40	0.14	0.11	0.02	0.12
9H-1, 70–71	23.70	0.13	0.10	0.02	0.12
10H-1, 83–84	27.13	0.12	0.10	0.03	0.12
10H-2, 83–84	28.63	0.12	0.06	0.06	0.11
11H-2, 65–66	31.45	0.12	0.08	0.04	0.11
13H-1, 88–89	33.48	0.11	0.07	0.04	0.12
13H-2, 88–89	34.98	0.15	0.11	0.04	0.13
347-M0062B-					
2H-1, 71–72	1.71	0.70	0.62	0.08	0.13
2H-2, 71–72	3.21	0.72	0.70	0.02	0.10
3H-1, 29–30	4.59	0.85	0.83	0.02	0.14
4H-1, 42–43	8.02	1.31	1.30	0.02	1.02
4H-2, 102–103	10.12	0.78	0.78	0.00	0.07
5H-1, 42–44	11.32	0.81	0.81	0.00	0.10
5H-2, 120–121	13.60	0.32	0.31	0.01	0.13
6H-2, 68–69	16.38	0.16	0.13	0.04	0.13
7H-2, 38–39	19.38	0.13	0.11	0.01	0.12
8H-1, 48–49	21.28	0.14	0.14	0.00	0.13
347-M0062C-					
1H-1, 68–69	0.68	1.25	1.14	0.11	0.23
1H-2, 103–104	2.53	0.79	0.69	0.10	0.12
347-M0062D-					
2H-1, 40.5–42	1.91	0.84	0.68	0.16	0.14
3H-1, 100–101.5	5.80	1.11	1.08	0.03	0.37
4H-1, 30–31	8.40	1.29	1.19	0.10	1.02
4H-2, 81–82	10.41	0.54	0.51	0.03	0.31
5H-1, 30–31	11.70	0.87	0.84	0.03	0.11
5H-2, 117–118	14.06	0.24	0.13	0.11	0.13
6H-1, 30–31	15.00	0.18	0.10	0.08	0.13
6H-2, 112–113	17.32	0.21	0.17	0.03	0.13
7H-1, 40–41	18.10	0.15	0.23	0.00	0.14
7H-2, 102–103	20.21	0.12	0.02	0.09	0.11

Table T7. Composite depth scale, Site M0062.

Core	Offset (m)	Top depth (mbsf)	Top depth (mcd)
347-M0062A-			
2H	0.00	0.5	0.50
3H	0.00	3.8	3.80
4H	0.00	7.1	7.10
5H	0.38	10.4	10.78
6H	0.38	13.7	14.08
7H	0.38	16.4	16.78
8H	0.83	19.7	20.53
9H	0.83	23.0	23.83
10H	0.83	26.3	27.13
11H	0.83	29.3	30.13
13H	0.83	32.6	33.43
347-M0062B-			
2H	0.00	1.0	1.00
3H	0.04	4.3	4.34
4H	0.39	7.6	7.99
5H	0.39	10.9	11.29
6H	0.39	14.2	14.59
7H	0.30	17.5	17.80
8H	0.30	20.8	21.10
347-M0062C-			
1H	–0.36	0.0	–0.36
347-M0062D-			
2H	0.25	1.5	1.75
3H	–0.17	4.8	4.63
4H	–0.14	8.1	7.96
5H	0.15	11.4	11.55
6H	0.41	14.7	15.11
7H	0.34	17.7	18.04

Table T8. Splice tie points, Site M0062.

Hole, core, section, interval (cm)	Depth (mbsf)	Depth (mcd)		Hole, core, section, interval (cm)
347-				347-
M0062C-1H-2, 61	1.75	1.75	Tie to	M0062A-2H-1, 125
M0062A-2H-2, 115	2.90	3.15	Tie to	M0062D-2H-1, 140
M0062D-2H-3, 9	4.84	4.84	Tie to	M0062A-3H-1, 104
M0062A-3H-2, 101	6.48	6.31	Tie to	M0062D-3H-2, 17
M0062D-3H-3, 7	7.71	7.71	Tie to	M0062A-4H-1, 61
M0062A-4H-2, 124	9.98	9.84	Tie to	M0062D-4H-2, 37
M0062D-4H-4, 8	10.81	11.19	Tie to	M0062A-5H-1, 40
M0062A-5H-1, 134	11.98	12.13	Tie to	M0062D-5H-1, 57
M0062D-5H-2, 147	14.14	14.52	Tie to	M0062A-6H-1, 44
M0062A-6H-2. 89	16.07	16.48	Tie to	M0062D-6H-1, 137
M0062D-6H-2, 75	16.98	17.36	Tie to	M0062A-7H-1, 44
M0062A-7H-2, 71	18.66	19.00	Tie to	M0062D-7H-1, 95
M0062D-7H-3, 21	20.11	20.94	Tie to	M0062A-8H-1, 41
M0062A-8H-3, 12	23.07	23.90	Append	M0062A-9H-1, 7
M0062A-9H-2, 144	26.37	27.20	Append	M0062A-10H-1, 7
M0062A-10H-2, 114	29.36	30.19	Append	M0062A-11H-1, 6
M0062A-11H-3, 11	32.68	33.51	Append	M0062A-13H-1, 8

Table T9. Sound velocity data for lithostratigraphic units, Site M0062.

Unit	Thickness of unit (m)	Sound velocity (m/s)*	TWT (ms)	Depth (m)	Depth (mbsf)
Water column	68	1430	0.095	68.00	0.00
Ia	10.72	1445	0.110	78.72	10.72
Ib	5.45	1512	0.117	84.17	16.17
II	19.73	1461	0.144	103.90	35.90

* = sound velocities are based on values measured during the OSP. TWT = two-way traveltime.